Transport coefficients for granular gases of electrically charged particles in the homogeneous cooling state

Satoshi Takada[1]†, Dan Serero[2], and Thorsten Pöschel[2]

[1]Institute of Engineering, Tokyo University of Agriculture and Technology, 2–24–16, Naka-cho, Koganei, Tokyo 184–8588, Japan

[2]Lehrstuhl für Multiscale Simulation, Friedrich-Alexander-Universität Erlangen-Nürnberg, Cauerstraße 3, 91058 Erlangen, Germany

(Received xx; revised xx; accepted xx)

We consider a dilute gas of electrically charged granular particles in the homogeneous cooling state. We derive the energy dissipation rate and the transport coefficients from the inelastic Boltzmann equation. We find that the deviation of the velocity distribution function from the Maxwellian yields overshoots of the transport coefficients, and especially, the negative peak of the coefficient μ in the intermediate temperature regime. We perform the linear stability analysis and investigate the temperature dependence of each mode, where the instability mode is found to change against the temperature. The molecular dynamics simulations are also performed to compare the result with that from the kinetic theory.

Key words:

1. Introduction

Dilute granular gases have been subject of intensive research in the past decades and by now there is a large body of knowledge regarding the fluid mechanical and kinetic properties of granular gases, see e.g. Garzó (2019); Puglisi (2015); Brilliantov & T. Pöschel (2004); Goldhirsch (2003); Pöschel & Brilliantov (2003) and many references therein. There is an obvious similarity of ordinary molecular gases and granular gases which allows to apply the mathematical toolbox of statistical physics and kinetic theory also to granular gases, however, modifications are needed to account for the loss of mechanical energy due to dissipative particle collisions. The irreversible transfer of energy from the mechanical degrees of freedom on the particle level to the thermal (sub-particular) degrees of freedom is characterized by the coefficient of restitution, e, defined as the ratio between the normal components of the pre-collisional and post-collisional relative velocities of the colliding grains. In the absence of external driving mechanisms, therefore, the kinetic energy of granular gases decays monotonously. For the case of a homogeneous granular gas and for a constant coefficient of restitution, this decay is described by Haff's law Haff (1983) predicting decay of energy with time $\propto t^{-2}$. Similar results apply to gases of viscoelastic particles characterized by an impact velocity dependent coefficient of restitution Brilliantov *et al.* (1996) where energy decays $\propto t^{-5/3}$ Schwager & Pöschel

† Email address for correspondence: takada@go.tuat.ac.jp

(2008). The dissipative nature of particle interaction implies that granular gases are always in non-equilibrium, which gives rise to many interesting phenomena, such as non-Maxwellian velocity distribution Goldhirsch *et al.* (2003), over-population of the high-energy tail of the velocity distribution function Esipov & Pöschel (1997) or the instability of the homogeneous state in the long-time evolution Goldhirsch & Zanetti (1993) which may be transient, depending on the particle characteristics Brilliantov *et al.* (2004).

Much less is know when it comes to granular gases of electrically charged particles, despite the fact, that for many applications of practical interest it is known that electrical charges have significant influence or even dominate their macroscopic behavior, e.g., (Kumar *et al.* 2014; Laurentie *et al.* 2013; Lee *et al.* 2015; Jungmann *et al.* 2018). Systems of charges particles – mostly due to triboelectricity – are not only ubiquitous in industrial processes (Kanazawa *et al.* 1995; Watanabe *et al.* 2007), but also in natural phenomena such as volcanic eruptions (Genareau *et al.* 2015) and in protoplanetary discs (Muranushi 2010). Although the triboelectric effect has been known since ancient times, the underlying physics is still the subject of intense scientific debate, e.g. Pan & Zhang (2019); Lacks & Shinbrot (2019). Some recent work on this phenomenon can be found in (Kolehmainen *et al.* 2016; Yoshimatsu *et al.* 2017; Singh & Mazza 2018, 2019).

The presence of charges changes the collisional behavior of granular particles significantly: For uncharged particles, the properties of a collision are independent of the unit of time. Particle interactions are instantaneous events resulting in a change of the particle velocities due to a collision rule. Independent of the incoming velocity, the absolute value of the relative particle velocity (in normal direction) reduces by a fraction described by the coefficient of restitution. This is different for charged particles. Here, a dissipative collision can only occur if the particles overcome an energy barrier induced by the electrical charges. In contrast to Haff's law, the kinetic energy decays $\propto \log^{-1}(t)$ rather than $\propto t^{-\alpha}$ Scheffler & Wolf (2002). The same result with somewhat different reasoning was obtained in Pöschel *et al.* (2003). For both results, a Maxwellian velocity distribution was assumed. While this assumption simplifies the algebra significantly, it ignores pronounced deviations from the Maxwellian as a consequence of inelastic collisions Goldshtein & Shapiro (1995); van Noije & Ernst (1998); Brey *et al.* (1998); Brilliantov & Pöschel (2000); Goldhirsch *et al.* (2003). When taking these deviations into account (Takada *et al.* 2017), the functional form of the earlier result was reproduced, but the parameters and details are modified. That is, in the homogeneous cooling state of charged granular gases, initially the evolution of the granular temperature follows the Haff's law (Haff 1983) followed by a later stage where the evolution follows the inverse of the logarithm of time.

In the current paper, we continue the description of granular gases of charged particles by deriving the transport coefficients and in particular their dependence on temperature. We perform a linear stability analysis of the homogeneous cooling state and find that the route to instability of a granular gas of charged particles differs from the route of uncharged particles: For large temperature, the sound mode is stable and the heat mode is unstable for small wave number, similar to granular gases of uncharged particles. For small temperature, the heat mode becomes stable and the sound mode becomes unstable for small wave number. This behavior is not observed for uncharged gases. Instead, the shear mode is always dominant compared to the heat mode (Brey *et al.* 1998; Brilliantov & T. Pöschel 2004).

For our analysis, we assume a dilute granular gas, that is, small volume fraction of the particles. An extension to moderately dense systems would require an expression for the pair correlation function, which is, however, unknown for granular particles carrying charges.

In the next section, we calculate the transport coefficients. In Section 3, we perform the linear stability analysis for this system, and study the result in dependence on temperature. Finally, in Sec. 4, we perform numerical simulations to validate the theoretical results. Some extensive calculations have been moved to appendices so as not to disturb the flow of reading: in Appendix A, we determine the Sonine coefficients a_2 and a_3 from the Boltzmann equation. Appendix B describes the derivation of Ω_η^e and Ω_κ^e needed for the transport coefficients. Finally, in Appendix C, we explain the numerical method to compute the transport coefficients.

2. Kinetic theory and transport coefficients

2.1. *General method for the computation of transport coefficients*

We consider a system of monodisperse particles of mass m and diameter σ. The coefficient of restitution , e, depends on the impact velocity via (Takada *et al.* 2017)

$$e(v_n) = \frac{e^* \exp\left[\beta(v_n - v^*)\right] + 1}{\exp\left[\beta(v_n - v^*)\right] + 1}, \tag{2.1}$$

where e^* is the restitution coefficient for inelastic collision, v_n is the normal component if the relative velocity, v^* is the characteristic velocity, and β is related to the slope of the change near v^* (see Fig. 1 of Ref. (Takada *et al.* 2017)). Function (2.1) takes into account that for $v \ll v^*$ the particles collide elastically, due to the repulsive charges. For $v \gg v^*$ the collision takes place as for uncharged particles, due to the coefficient of restitution e^* since inertia dominates the collision. For $\beta \to \infty$, we recover the step-function used by Pöschel *et al.* (2003),

$$\lim_{\beta\to\infty} e(v_n) = 1 - \Theta(v_n - v^*)(1 - e^*), \tag{2.2}$$

where $\Theta(x)$ is the Heaviside function. In the homogeneous cooling state, the temperature of the system decays due of inelastic collisions. This decay can be obtained from the Boltzmann equation (Brilliantov & T. Pöschel 2004) as

$$\frac{dT}{dt} = -\frac{2}{3} n\sigma^2 g_2(\sigma)\sqrt{\frac{2T}{m}}\mu_2 T, \tag{2.3}$$

where n is the particle number density of the system, $g_2(\sigma)$ is the radial distribution function at contact, and the μ_2 is the second moment of the dimensionless collision integral. We expand the distribution function in terms of Sonine polynomials up to third order:

$$\tilde{f}(\boldsymbol{c}) = \phi(c)\left[1 + a_2 S_2(c^2) + a_3 S_3(c^2)\right], \tag{2.4}$$

where $\boldsymbol{c}$ is the dimensionless velocity $\boldsymbol{c} = \boldsymbol{v}/\sqrt{2T/m}$, $c = |\boldsymbol{c}|$, $\tilde{f}$ is the dimensionless velocity distribution function, $\phi(c)$ is the dimensionless Maxwell distribution function $\phi(c) = \pi^{-3/2}\exp(-c^2)$, and $S_p(x)$ $(p = 2, 3)$ are Sonine polynomials defined as (Brilliantov & T. Pöschel 2004; Chamorro *et al.* 2013)

$$S_p(x) = \sum_{n=0}^{p} \frac{(-1)^n\left(\frac{1}{2} + p\right)!}{\left(\frac{1}{2} + n\right)!(p-n)!} x^p. \tag{2.5}$$

For μ_2, we obtain (Takada *et al.* 2017)

$$\mu_2 = \sqrt{2\pi}(S_1 + a_2 S_2 + a_3 S_3), \tag{2.6}$$

where the explicit forms of S_1, S_2, and S_3 are, respectively, given in Appendix A, Eqs. (A 5a)–(A 5c). Similarly, we obtain the higher moments of the dimensionless collision integral:

$$\mu_4 = \sqrt{2\pi}(T_1 + a_2 T_2 + a_3 T_3), \tag{2.7}$$

$$\mu_6 = \sqrt{2\pi}(D_1 + a_2 D_2 + a_3 D_3), \tag{2.8}$$

where T_1, T_2, T_3, D_1, D_2, and D_3 are, respectively, given in Appendix A, Eqs. (A 6a)–(A 7c). Exploiting the properties of the collision integral, we can determine the coefficients a_2 and a_3 in linear approximation as

$$a_2 = \frac{N_2}{D}, \quad a_3 = \frac{N_3}{D}, \tag{2.9}$$

with

$$N_2 \equiv (T_1 - 5S_1)\left(-\frac{105}{4}S_1 + \frac{105}{4}S_3 - D_3\right) - (5S_3 - T_3)\left(D_1 - \frac{105}{4}S_1\right), \tag{2.10a}$$

$$N_3 \equiv (5S_1 + 5S_2 - T_2)\left(D_1 - \frac{105}{4}S_1\right) - (T_1 - 5S_1)\left(\frac{315}{4}S_1 + \frac{105}{4}S_2 - D_2\right), \tag{2.10b}$$

$$\begin{aligned} D \equiv{}& (5S_1 + 5S_2 - T_2)\left(-\frac{105}{4}S_1 + \frac{105}{4}S_3 - D_3\right) \\ &- (5S_3 - T_3)\left(\frac{315}{4}S_1 + \frac{105}{4}S_2 - D_2\right). \end{aligned} \tag{2.10c}$$

(The detailed derivation is provided in Appendix A.)

Now, let us derive the transport coefficients. Using the same procedure as the Chapman-Enskog method, we define

$$\begin{aligned} \Omega_\eta^e \equiv{}& \int d\boldsymbol{c}_1 \int d\boldsymbol{c}_2 \int d\hat{\boldsymbol{k}} \Theta(-\boldsymbol{c}_{12}\cdot\hat{\boldsymbol{k}}) \left|\boldsymbol{c}_{12}\cdot\hat{\boldsymbol{k}}\right| \phi(c_1)\phi(c_2) \\ &\times \left[1 + a_2 S_2(c_1^2) + a_3 S_3(c_1^2)\right] \widetilde{D}_{\alpha\beta}(\boldsymbol{c}_2) \Delta\left[\widetilde{D}_{\alpha\beta}(\boldsymbol{c}_1) + \widetilde{D}_{\alpha\beta}(\boldsymbol{c}_2)\right], \end{aligned} \tag{2.11}$$

with (Brilliantov & T. Pöschel 2004)

$$\widetilde{D}_{\alpha\beta}(\boldsymbol{c}) \equiv c_\alpha c_\beta - \frac{1}{3}c^2\delta_{\alpha\beta}\,. \tag{2.12}$$

Greek characters $\{\alpha, \beta\}$ stand for $\{x, y, z\}$, and we adopt Einstein's rule for the summation. Substituting Eq. (2.1) into Eq. (2.11), we obtain

$$\Omega_\eta^e = \sqrt{2\pi}(\omega_{\eta,1}^e + a_2\omega_{\eta,2}^e + a_3\omega_{\eta,3}^e), \tag{2.13}$$

where $\Omega_{\eta,1}^e$, $\Omega_{\eta,2}^e$, and $\Omega_{\eta,3}^e$ are, respectively, given in Appendix B, Eqs. (B 5a)–(B 5d).

Similarly, we define

$$\begin{aligned} \Omega_\kappa^e \equiv{}& \int d\boldsymbol{c}_1 \int d\boldsymbol{c}_2 \int d\hat{\boldsymbol{k}} \Theta(-\boldsymbol{c}_{12}\cdot\hat{\boldsymbol{k}}) \left|\boldsymbol{c}_{12}\cdot\hat{\boldsymbol{k}}\right| \phi(c_1)\phi(c_2) \\ &\times \left[1 + a_2 S_2(c_1^2) + a_3 S_3(c_1^2)\right] \widetilde{\boldsymbol{S}}(\boldsymbol{c}_2) \Delta\left[\widetilde{\boldsymbol{S}}(\boldsymbol{c}_1) + \widetilde{\boldsymbol{S}}(\boldsymbol{c}_2)\right], \end{aligned} \tag{2.14}$$

with (Brilliantov & T. Pöschel 2004)

$$\widetilde{\boldsymbol{S}} \equiv \left(c^2 - \frac{5}{2}\right)\boldsymbol{c}\,. \tag{2.15}$$

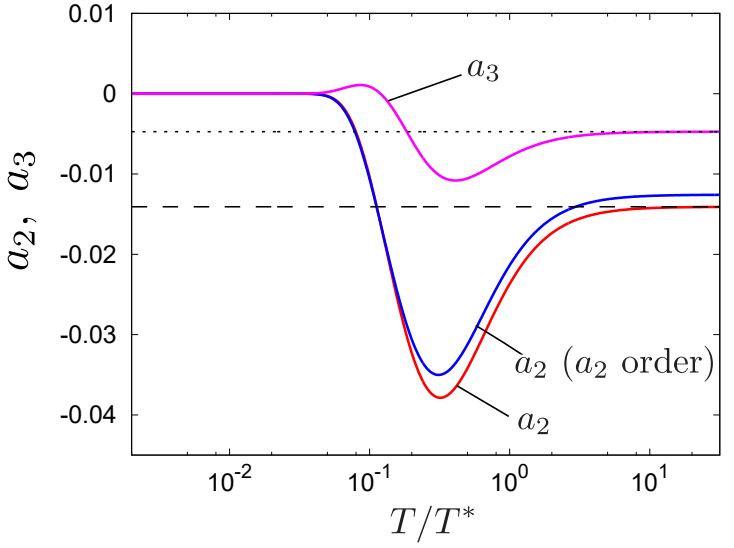

FIGURE 1. The temperature dependence of the coefficients a_2 and a_3 up to a_3 order for $e^* = 0.8$. We also show a_2 up to a_2 order for $e^* = 0.8$. The dashed (dotted) lines show a_2 (a_3) for a hard-sphere gas with $e^* = 0.8$ whose explicit form is given by Eq. (2.18).

We obtain

$$\Omega_\kappa^e = \sqrt{2\pi}(\omega_{\kappa,1}^e + a_2\omega_{\kappa,2}^e + a_3\omega_{\kappa,3}^e), \tag{2.16}$$

where $\Omega_{\kappa,1}^e$, $\Omega_{\kappa,2}^e$, and $\Omega_{\kappa,3}^e$ are, respectively, given in Appendix B, Eqs. (B 8*a*)–(B 8*c*).

2.2. *Discontinuous limit of the restitution coefficient*

Consider the transport coefficients in the discontinuous limit, $\beta v^* \to \infty$. In this limit, Eqs. (2.6)–(2.8), (2.13), and (2.16) read

$$\mu_2^{(\infty)} = \sqrt{2\pi}\left(S_1^{(\infty)} + a_2^{(\infty)}S_2^{(\infty)} + a_3^{(\infty)}S_3^{(\infty)}\right), \tag{2.17a}$$

$$\mu_4^{(\infty)} = \sqrt{2\pi}\left(T_1^{(\infty)} + a_2^{(\infty)}T_2^{(\infty)} + a_3^{(\infty)}T_3^{(\infty)}\right), \tag{2.17b}$$

$$\mu_6^{(\infty)} = \sqrt{2\pi}\left(D_1^{(\infty)} + a_2^{(\infty)}D_2^{(\infty)} + a_3^{(\infty)}D_3^{(\infty)}\right), \tag{2.17c}$$

$$\Omega_\eta^{e(\infty)} = \sqrt{2\pi}\left(\omega_{\eta,1}^{e(\infty)} + a_2^{(\infty)}\omega_{\eta,2}^{e(\infty)} + a_3^{(\infty)}\omega_{\eta,3}^{e(\infty)}\right), \tag{2.17d}$$

$$\Omega_\kappa^{e(\infty)} = \sqrt{2\pi}\left(\omega_{\kappa,1}^{e(\infty)} + a_2^{(\infty)}\omega_{\kappa,2}^{e(\infty)} + a_3^{(\infty)}\omega_{\kappa,3}^{e(\infty)}\right), \tag{2.17e}$$

whose explicit forms are given in Appendices A and B. Hereafter, we focus on the discontinuous limit $\beta v^* \to \infty$; we drop the superscript (∞) for simplicity.

Let us start with the coefficients a_2 and a_3. Figure 1 shows a_2 and a_3 as functions of temperature given by Eqs. (2.9) in the limit $\beta v^* \to \infty$. In the Figure, we have introduced the characteristic temperature, $T^* \equiv m v^{*2}/2$, given by the characteristic velocity v^* (Takada *et al.* 2017). We also show a_2 up to the second term in Eq. (2.4), whose explicit form is given in (Takada *et al.* 2017), Eq. (10). We find that the high temperature limit is consistent with the corresponding value for a hard-sphere gases, where $a_2^{(\mathrm{HC})}$ and $a_3^{(\mathrm{HC})}$

are, respectively, given by (Brilliantov & Pöschel 2006):

$$a_2^{(\mathrm{HC})}(e^*) \equiv \frac{N_2^{(\mathrm{HC})}(e^*)}{D^{(\mathrm{HC})}(e^*)}, \tag{2.18a}$$

$$a_3^{(\mathrm{HC})}(e^*) \equiv \frac{N_3^{(\mathrm{HC})}(e^*)}{D^{(\mathrm{HC})}(e^*)}, \tag{2.18b}$$

with

$$\begin{aligned} N_2^{(\mathrm{HC})}(e^*) \equiv 16\big(&1623 - 1934e^* - 895e^{*2} + 364e^{*3} - 3510e^{*4} \\ &+7424e^{*5} - 3312e^{*6} + 480e^{*7} - 240e^{*8}\big), \end{aligned} \tag{2.19a}$$

$$\begin{aligned} N_3^{(\mathrm{HC})}(e^*) \equiv -128\big(&217 - 386e^* - 669e^{*2} + 1548e^{*3} + 154e^{*4} \\ &-1600e^{*5} + 816e^{*6} - 160e^{*7} + 80e^{*8}\big), \end{aligned} \tag{2.19b}$$

$$\begin{aligned} D^{(\mathrm{HC})}(e^*) \equiv &214357 - 172458e^* + 112155e^{*2} + 25716e^{*3} - 4410e^{*4} \\ &- 84480e^{*5} + 34800e^{*6} - 5600e^{*7} + 2800e^{*8}. \end{aligned} \tag{2.19c}$$

The coefficient a_3 has both minimum and maximum in the intermediate regime, while a_2 has only a minimum in this regime. The position of the minimum of a_3 coincides almost with the position of the minimum of a_2. From Eq. (2.3), the dissipation rate ζ is written as

$$\zeta = \frac{2}{3} n\sigma^2 g_2(\sigma)\sqrt{\frac{2T}{m}}\mu_2. \tag{2.20}$$

Figure 2 shows the dissipation rate as a function of temperature. Here, we introduce a new variable

$$\zeta^* \equiv \frac{\zeta}{\zeta^{(\mathrm{HC})}(e^*)} \tag{2.21}$$

where

$$\zeta^{(\mathrm{HC})}(e^*) = \frac{4}{3}\left(1 - e^{*2}\right) n\sigma^2 g_2(\sigma)\sqrt{\frac{\pi T}{m}}\mu_2^{(\mathrm{HC})}\left(1 + \frac{3}{16}a_2^{(\mathrm{HC})}(e^*) + \frac{1}{64}a_3^{(\mathrm{HC})}(e^*)\right). \tag{2.22}$$

In the limit of high temperature, the dissipation rate is consistent with the hard-sphere limit while it decreases to zero as the temperature becomes sufficiently smaller than the characteristic temperature.

Next, we consider the shear viscosity, η, as a function of temperature, using the technique introduced in (Takada *et al.* 2016). Then, the shear viscosity is given by the solution of the differential equation

$$-\frac{2}{3}T\mu_2\frac{\partial\eta}{\partial T} - \frac{2}{5}\Omega_\eta^e\eta = \frac{1}{\sigma^2 g_2(\sigma)}\sqrt{\frac{mT}{2}}. \tag{2.23}$$

Here, we define a new variable

$$\eta^* \equiv \frac{\eta}{\eta^{(\mathrm{HC})}(1)} \quad \text{where} \quad \eta^{(\mathrm{HC})}(1) = \frac{5}{16\sigma^2 g_2(\sigma)}\sqrt{\frac{mT}{\pi}} \tag{2.24}$$

is the shear viscosity of the elastic hard-sphere gas. Using η^*, Eq. (2.23) reads

$$10x\mu_2\frac{\partial\eta^*}{\partial x} - \left(5\mu_2 + 6\Omega_\eta^e\right)\eta^* = 24\sqrt{2\pi}. \tag{2.25}$$

To solve this equation perturbatively, we expand $\eta^* = \eta^{*(0)} + \eta^{*(1)} + \cdots$ and assume

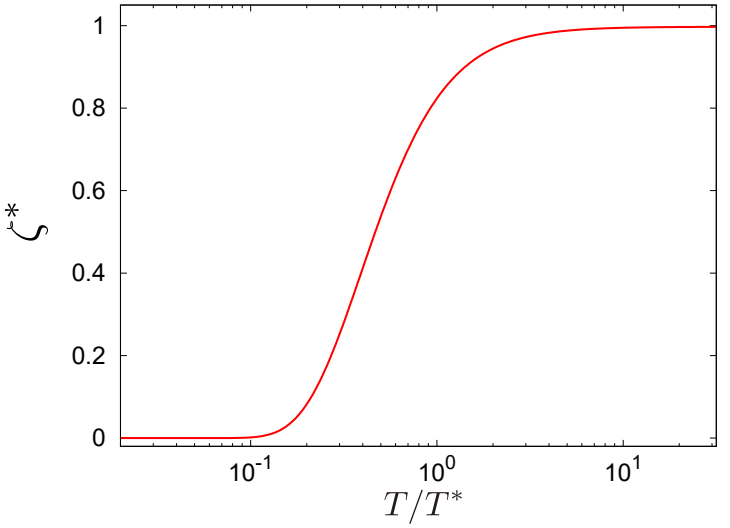

FIGURE 2. Dissipation rate as a function of temperature, obtained from the kinetic theory up to order a_3 for $e^* = 0.8$, where ζ^* is given by Eq. (2.21).

that the first term of the left-hand side of Eq. (2.25) is of higher order than the other terms. See below for a discussion of this assumption. Then we can perturbatively solve Eq. (2.25):

$$\eta^* = \sum_{n=0}^{\infty} \eta^{*(n)} = \sum_{n=0}^{\infty} \left(\frac{10x\mu_2}{5\mu_2 + 6\Omega_\eta^e} \frac{\partial}{\partial x} \right)^n \eta^{*(0)}, \tag{2.26}$$

with

$$x \equiv \frac{T^*}{2T} \qquad \text{and} \qquad \eta^{*(0)} = -\frac{24\sqrt{2\pi}}{5\mu_2 + 6\Omega_\eta^e}. \tag{2.27}$$

Note that

$$\frac{\partial}{\partial x} = -\frac{2T^2}{T^*} \frac{\partial}{\partial T} \tag{2.28}$$

holds true. Figure 3 shows the shear viscosity as a function of temperature, Eq. (2.26), up to the first order. In the limit of high temperature, we recover the result for an inelastic hard-sphere gas while for low temperature we find the result for the elastic hard-sphere gas. This agrees with the intuition that for high temperature nearly all collisions are dissipative while for low temperature elastic collisions dominate. In the intermediate region, we obtain a negative overshoot around $T/T^* \simeq 0.1$. This behavior is also observed when we assume a Maxwell distribution function (not shown in Fig. 3). We also show the numerical solution of the differential equation (2.25); details are discussed in Appendix C. The numerical result is consistent with the perturbative solution, that is, the numerics supports the validity of the theoretical result.

Similarly, the thermal conductivity and the coefficient μ are, respectively, given by the solutions of the differential equations:

$$\frac{\partial}{\partial T}\left(4\mu_2\kappa T^{3/2}\right) + \frac{8}{5}\kappa T^{1/2}\Omega_\kappa^e = -\frac{15}{2}\frac{T}{\sigma^2 g_2(\sigma)}\sqrt{\frac{2}{m}}(1+2a_2), \tag{2.29}$$

$$-4\mu_2\frac{\partial \mu}{\partial T} - \frac{8}{5}T^{-1}\Omega_\kappa^e\mu = \frac{4}{n}\mu_2\kappa + a_2\frac{15}{2n\sigma^2 g_2(\sigma)}\sqrt{\frac{2T}{m}}. \tag{2.30}$$

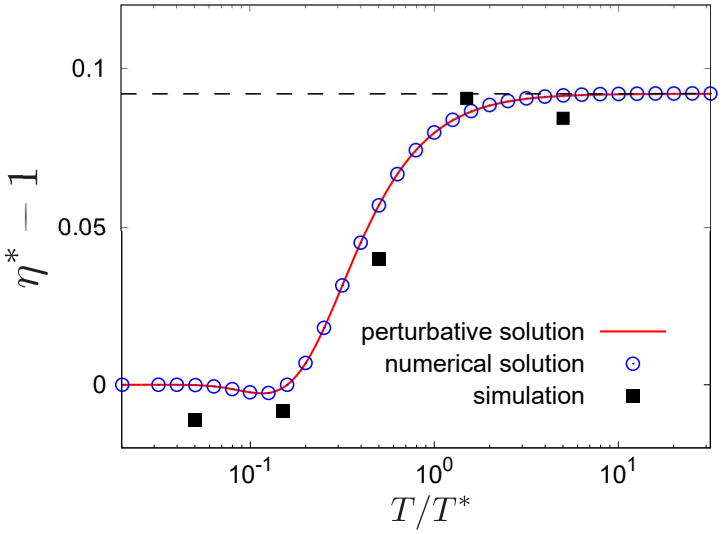

FIGURE 3. Shear viscosity as a function of temperature obtained from the kinetic theory up to a_3 order (solid line) and that up to a_2 (open circles) order for $e^* = 0.8$, where η^* is given by Eq. (2.24). The filled squares show the simulation results. The dashed line is the shear viscosity of a hard-sphere gas, $\eta^{(\mathrm{HC})}(e^*)$, (Eq. (C 2)).

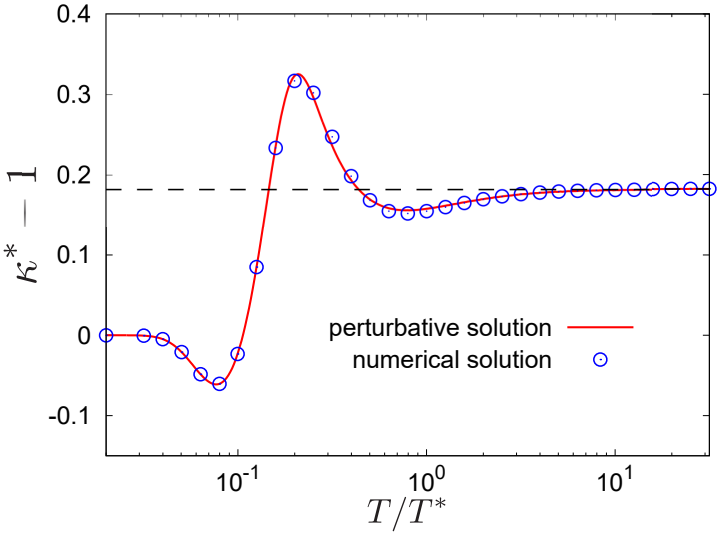

FIGURE 4. Thermal conductivity as a function of temperature, obtained from the kinetic theory up to order a_3 (solid line) and up to order a_2 (open circles) for $e^* = 0.8$, where κ^* is given by Eq. (2.31). The dashed line is the thermal conductivity of hard-sphere gases $\kappa^{(\mathrm{HC})}(e^*)$ (Eq. (C 8)).

Introducing new variables

$$\kappa^* \equiv \frac{\kappa}{\kappa^{(\mathrm{HC})}(1)} \qquad \text{and} \qquad \mu^* = \frac{\frac{n\mu}{T}}{\kappa^{(\mathrm{HC})}(1)} \tag{2.31}$$

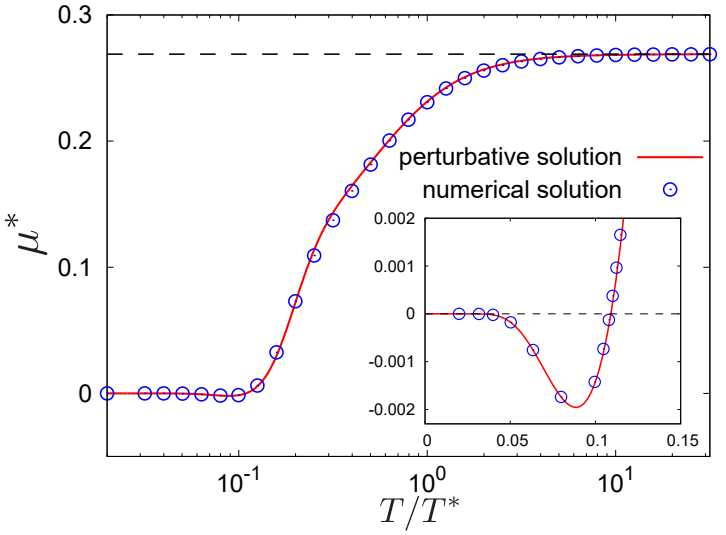

FIGURE 5. The temperature dependence of the coefficient μ obtained from the kinetic theory up to a_3 order (solid line) and that up to a_2 order (open circles) for $e^* = 0.8$, where μ^* is given by Eq. (2.31). The dashed line shows the result for an inelastic hard-sphere gas, $n\mu^{(\mathrm{HC})}(e^*)/(\kappa^{(\mathrm{HC})}(1)T)$ (Eq. (C 9)). The inset shows a magnification of the intermediate regime.

with the thermal conductivity of the elastic hard-sphere gas

$$\kappa^{(\mathrm{HC})}(1) = \frac{75}{64\sigma^2 g_2(\sigma)}\sqrt{\frac{T}{\pi m}}, \tag{2.32}$$

we can rewrite Eqs. (2.29) and (2.30):

$$5x\mu_2\frac{\partial\kappa^*}{\partial x} - \left(10\mu_2 - 5x\frac{\partial\mu_2}{\partial x} + 2\Omega_\kappa^e\right)\kappa^* = 8\sqrt{2\pi}(1+2a_2), \tag{2.33}$$

$$10x\mu_2\frac{\partial\mu^*}{\partial x} - (15\mu_2 + 4\Omega_\kappa^e)\,\mu^* = 2\mu_2\kappa^* + 16\sqrt{2\pi}a_2\,. \tag{2.34}$$

Similar to the shear viscosity, we can perturbatively obtain the solutions as

$$\kappa^* = \sum_{n=0}^{\infty}\kappa^{*(n)} = \sum_{n=0}^{\infty}\left(\frac{5x\mu_2}{10\mu_2 - 5x\mu_2' + 2\Omega_\kappa^e}\frac{\partial}{\partial x}\right)^n\kappa^{*(0)}, \tag{2.35}$$

$$\mu^* = \sum_{n=0}^{\infty}\mu^{*(n)} = \sum_{n=0}^{\infty}\left(\frac{10x\mu_2}{15\mu_2 + 4\Omega_\kappa^e}\frac{\partial}{\partial x}\right)^n\mu^{*(0)}, \tag{2.36}$$

respectively, with

$$\mu_2' = \partial\frac{\mu_2}{\partial x}, \tag{2.37}$$

$$\kappa^{*(0)} = -\frac{8\sqrt{2\pi}(1+2a_2)}{10\mu_2 - 5x\mu_2' + 2\Omega_\kappa^e}, \tag{2.38}$$

$$\mu^{*(0)} = -\frac{10\mu_2\kappa^* + 16\sqrt{2\pi}a_2}{15\mu_2 + 4\Omega_\kappa^e}. \tag{2.39}$$

Figures 4 and 5 show the thermal conductivity, Eq. (2.35), and the coefficient μ, Eq. (2.36), as functions of temperature. Again, the numerical solution supports the validity of the analytical results.

The thermal conductivity has both negative and positive peaks at around $T/T^* \simeq 0.1$ and 0.2, respectively. Similar to the shear viscosity, these peaks are found also when a Maxwell distribution function is assumed. The coefficient μ behaves similar to the shear viscosity, however, the value becomes negative in this region as shown in the inset of Fig. 5. This means that the heat flux is directed from dilute regions to dense regions. We will discuss this phenomenon below.

3. Linear stability analysis of the homogeneous cooling state

From the zeroth, first, and second moments of the Boltzmann equation, we obtain a set of hydrodynamic equations:

$$\frac{\partial n}{\partial t} + \boldsymbol{\nabla}\cdot(n\boldsymbol{u}) = 0, \tag{3.1a}$$

$$\frac{\partial \boldsymbol{u}}{\partial t} + \boldsymbol{u}\cdot\boldsymbol{\nabla}\boldsymbol{u} = -\frac{1}{nm}\boldsymbol{\nabla}p + \frac{\eta}{nm}\left[\nabla^2\boldsymbol{u} + \frac{1}{3}\boldsymbol{\nabla}(\boldsymbol{\nabla}\cdot\boldsymbol{u})\right], \tag{3.1b}$$

$$\frac{\partial T}{\partial t} + \boldsymbol{u}\cdot\boldsymbol{\nabla}T = -\zeta T + \frac{2}{3n}\left(\kappa\nabla^2 T + \mu\nabla^2 n\right) - \frac{2}{3n}p(\boldsymbol{\nabla}\cdot\boldsymbol{u}) + \frac{2}{3n}\eta\left[(\nabla_\alpha u_\beta)(\nabla_\beta u_\alpha) + (\nabla_\beta u_\alpha)(\nabla_\alpha u_\beta) - \frac{2}{3}(\boldsymbol{\nabla}\cdot\boldsymbol{u})^2\right], \tag{3.1c}$$

with the static pressure $p = nT$. We linearize the equations around the homogeneous cooling state,

$$n(\boldsymbol{r},t) = n_{\mathrm{H}} + \delta n \tag{3.2a}$$

$$T(\boldsymbol{r},t) = T_{\mathrm{H}} + \delta T, \tag{3.2b}$$

where the subscript H indicates the quantities due to the homogeneous system and consider only linear term with respect to

$$\rho \equiv \frac{\delta n}{n_{\mathrm{H}}}, \quad \boldsymbol{w} \equiv \frac{\boldsymbol{u}}{v_{\mathrm{T}}}, \quad \theta \equiv \frac{\delta T}{T_{\mathrm{H}}}, \tag{3.3}$$

with the thermal velocity $v_{\mathrm{T}} \equiv \sqrt{2T/m}$. We introduce dimensionless time and space variables, τ and $\hat{\boldsymbol{r}}$, by

$$\tau \equiv \int_0^t dt' \nu_{\mathrm{H}}(t'), \tag{3.4a}$$

$$\hat{\boldsymbol{r}} \equiv \frac{2\nu_{\mathrm{H}}(t)}{v_{\mathrm{T}}(t)}\boldsymbol{r}, \tag{3.4b}$$

with the collision frequency for the elastic hard-sphere gas

$$\nu_{\mathrm{H}} = \frac{16}{5}n\sigma^2 g_2(\sigma)\sqrt{\frac{\pi T}{m}}\,. \tag{3.5}$$

After linearization and Fourier transformation, the set of hydrodynamic equations becomes

$$\frac{\partial}{\partial\tau}\rho_{\rm k} = -ikw_{\rm k\|}, \tag{3.6a}$$

$$\frac{\partial}{\partial\tau}w_{\rm k\|} = -\frac{1}{2}ik\rho_{\rm k} + \left(\frac{1}{4}\zeta^* - \frac{4}{3}\eta^* k^2\right) w_{\boldsymbol{k}\|} - \frac{1}{2}ik\theta_{\rm k}, \tag{3.6b}$$

$$\frac{\partial}{\partial\tau}w_{\rm k\perp} = \left(\frac{1}{4}\zeta^* - \eta^* k^2\right) w_{\rm k\perp}, \tag{3.6c}$$

$$\frac{\partial}{\partial\tau}\theta_{\rm k} = \left(-\frac{1}{2}\zeta^* - \frac{5}{2}\mu^* k^2\right)\rho_{\rm k} - \frac{2}{3}ikw_{\rm k\|} + \left(-A\zeta^* - \frac{5}{2}\kappa^* k^2\right)\theta_{\rm k}, \tag{3.6d}$$

with

$$\zeta^* = \zeta\frac{\eta^{(\rm HC)}(1)}{nT} \tag{3.7}$$

and

$$A \equiv \frac{1}{4} + \frac{1}{2}T\frac{\partial}{\partial T}\log\mu_2 = \frac{1}{4} - \frac{1}{2}x\frac{\partial}{\partial x}\log\mu_2. \tag{3.8}$$

The variables $\Psi_{\rm k}(=\rho_{\rm k}, \boldsymbol{w}_{\rm k}, \theta_{\rm k})$ denote the Fourier component of the quantity Ψ:

$$\Psi_{\rm k}(\tau) = \int d\hat{\boldsymbol{r}}\Psi(\hat{\boldsymbol{r}},\tau)e^{-i\boldsymbol{k}\cdot\hat{\boldsymbol{r}}} \tag{3.9}$$

and $w_{\boldsymbol{k}\|}$ and $\boldsymbol{w}_{\boldsymbol{k}\perp}$ are the longitudinal and transversal components of the velocity field with respect to the wave vector $\boldsymbol{k}$.

Equation (3.6c) can be easily solved as

$$w_{\rm k\perp}(\tau) = w_{\rm k\perp}(0)\exp\left(\lambda_\perp\tau\right), \tag{3.10}$$

with

$$\lambda_\perp = \frac{1}{4}\zeta^* - \eta^* k^2, \tag{3.11}$$

and the threshold for this shear mode is given by

$$k_\perp = \frac{1}{2}\sqrt{\frac{\zeta^*}{\eta^*}}. \tag{3.12}$$

From Eqs. (3.6a), (3.6b), and (3.6d), other three eigenmodes λ_i $(i = 1, 2, 3)$ can be obtained as the solutions of the third-order equation

$$\begin{aligned}\lambda^3 + \left[\left(A - \frac{1}{4}\right)\zeta^* + \left(\frac{4}{3}\eta^* + \frac{5}{2}\kappa^*\right)k^2\right]\lambda^2 \\ + \left[-\frac{1}{4}A\zeta^{*2} + \left(\frac{5}{6} + \frac{4}{3}A\zeta^*\eta^* - \frac{5}{8}\zeta^*\kappa^*\right)k^2 + \frac{10}{3}\eta^*\kappa^* k^4\right]\lambda \\ + \left[\left(\frac{A}{2} - \frac{1}{4}\right)\zeta^* k^2 + \frac{5}{4}(\kappa^* - \mu^*)k^4\right] = 0.\end{aligned} \tag{3.13}$$

We can numerically obtain the thresholds for the heat mode and the sound modes from Eq. (3.13).

Figure 6 shows the wave number dependence of each mode. In the high-temperature regime, the real part of the heat mode becomes positive for small k, rendering the heat mode unstable. In contrast, the sound mode is stable for all k. For $T \simeq 1.6T^*$ and large k, the real parts of the heat mode are almost equal to those of the sound modes. For smaller

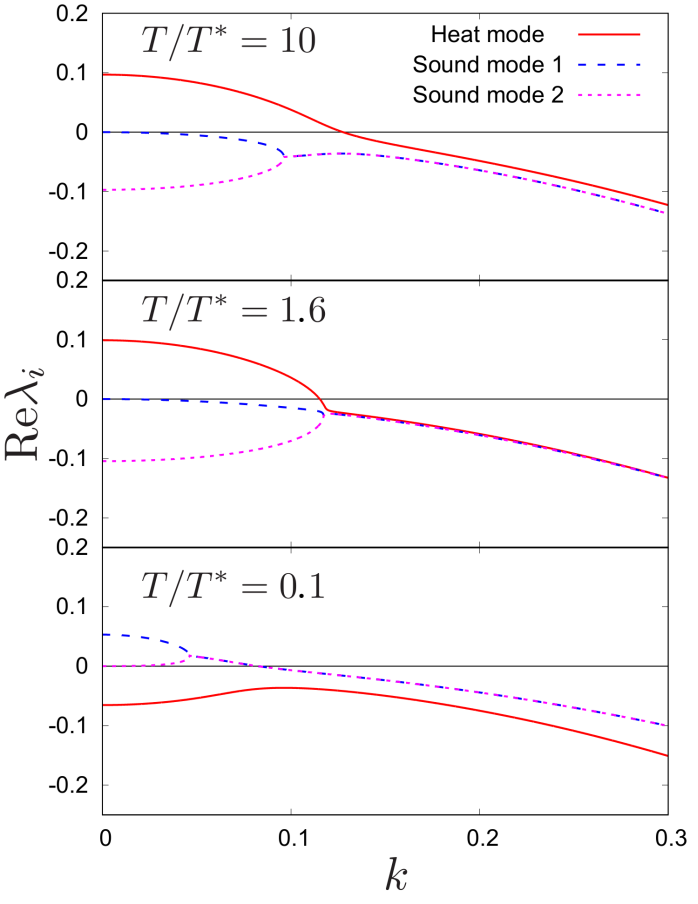

FIGURE 6. The wave number dependence of the real parts of the heat mode (solid line) and the sound mode (dashed and dotted lines) for $T/T^* = 10$, 1.6, and 0.1 and $e^* = 0.8$.

temperature, the real part of the heat mode is negative for all k and the real parts of the sound modes becomes positive for small k, which is not observed for hard-sphere gases. Figure 7 shows the temperature dependencies of the threshold values for the shear mode, the heat mode, and the sound mode, where k_h and k_s are the wave numbers where Eq. (3.13) is satisfied. In the high-temperature limit, both thresholds correspond to elastic or dissipative hard-sphere gases. On the other hand, the threshold for the heat mode becomes imaginary below $0.5T^*$, while that for the shear mode decreases to zero. Below $1.6T^*$, as shown in Fig. 6, the real part of the heat mode becomes negative while those of the sound modes become positive for small k. In addition, the threshold for the sound modes has a peak around $0.3T^*$.

4. Numerical confirmation of the results

In order to validate the theoretical results presented in the preceding Sections, we performed event-driven molecular dynamics simulations of the granular system. In particular, here we focus on the numerical measurement of the shear viscosity. Obviously, the shear viscosity in a system operating in the homogeneous cooling state is different from

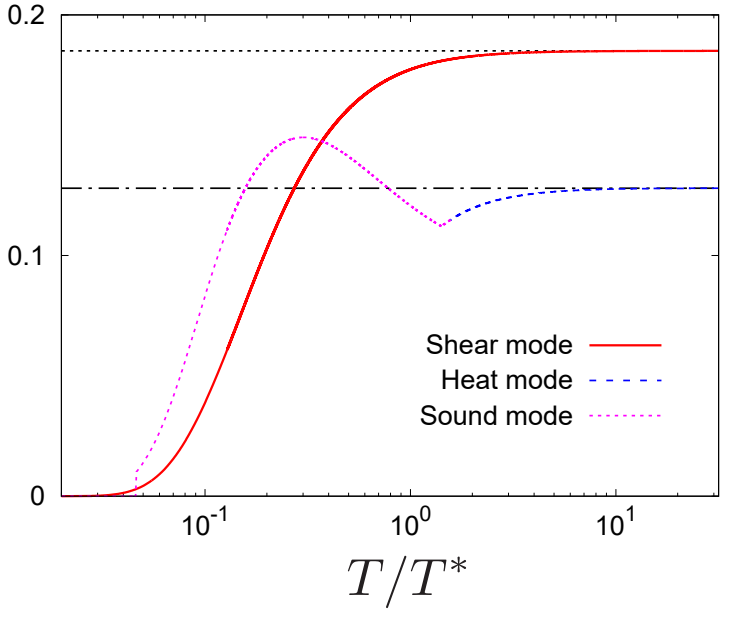

FIGURE 7. Threshold values of the shear mode (solid line), the heat mode (dashed line), and the sound modes (dotted line) as functions of the temperature for $e^* = 0.8$. The dotted black line shows the value of the shear mode for a hard-sphere gas. The dot-dashed line refers to the heat mode of a hard-sphere gas.

the shear viscosity in a uniformly sheared phase (Santos *et al.* 2004; Takada *et al.* 2016; Takada & Hayakawa 2018). Consequently, we must not determine numerically the value of shear viscosity in the traditional way. Instead, for systems in the homogeneous cooling state, Brey & Cubero (2001) introduced a protocol to determine the shear viscosity from a relaxation process, that is, a perturbation is added to the system and the relaxation is observed.

We consider a set of $N = 3,000$ particles of mass m and diameter σ homogeneously distributed in a cubic box of side length $L = 54\,\sigma$ with periodic boundary conditions. The given parameters correspond to a packing fraction of $\phi = 1.0 \times 10^{-2}$ (corresponding to the number density $n\sigma^3 \simeq 1.9 \times 10^{-2}$). We add a velocity perturbation via

$$u_y(x, t = 0) \propto \sin\left(\frac{2\pi}{L}x\right) \tag{4.1}$$

and observe the relaxation back to the uniform state in the course of time. Following Brey & Cubero (2001) and using Eqs. (3.3) and (3.10), the value of the shear viscosity, η^*, can be obtained from

$$u_y(x, t) \propto \exp\left(-\eta^* k^2 \tau\right). \tag{4.2}$$

Figure 3 (black square symbols) shows the shear viscosity determined by means of Eq. (4.2) in comparison with the theoretical results. In the whole range of the temperature, the result is consistent with the theory (2.26). Small deviations of the MD simulation data from the theory arise due to the statistical nature of the particle system (Brey & Cubero 2001).

Note that an MD numerical confirmation of the thermal conductivity and the coefficient μ in a granular system is much more complicated since these two coefficients are coupled (Dufty & Brey 2002; Brey & Ruiz-Montero 2004; Brey *et al.* 2005).

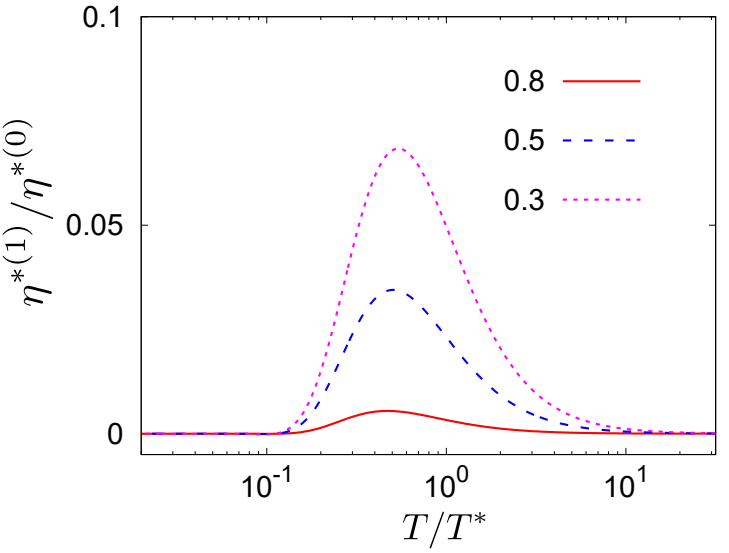

FIGURE 8. The ratio $\eta^{*(1)}$ to $\eta^{*(0)}$ of the first terms of Eq. (2.26) as a function of temperature for the restitution coefficient $e^* = 0.8$ (solid line), $e^* = 0.5$ (dashed line), and $e^* = 0.3$ (dotted line).

5. Discussion

To check the validity of the perturbative solution of Eq. (2.25) to derive the shear viscosity, we relate the first terms of Eq. (2.26) and obtain

$$\begin{aligned}\frac{\eta^{*(1)}}{\eta^{*(0)}} &= \frac{10x\mu_2}{5\mu_2 + 6\Omega_\eta^e}\frac{\partial}{\partial x}\log\eta^{*(0)} \\ &= -\frac{10x\mu_2}{(5\mu_2+6\Omega_\eta^e)^2}\left(5\frac{\partial\mu_2}{\partial x} + 6\frac{\partial\Omega_\eta^e}{\partial x}\right).\end{aligned} \tag{5.1}$$

Figure 8 this ratio as a function of the temperature for various values of the coefficient of restitution, e^*. Even for moderately large inelasticity, we obtain $\eta^{*(1)}/\eta^{*(0)} \ll 1$, justifying the perturbation solution.

Let us analyze the crossover temperature. We define the effective restitution coefficient $e_{\rm eff}$ (Takada *et al.* 2017) as

$$1 - e_{\rm eff}^2 = \left(1 - e^{*2}\right)(1+x)e^{-x}, \tag{5.2}$$

where the right-hand side of Eq. (5.2) is equivalent to S_1 for $\beta v^* \to \infty$ given by Eq. (A 10a). The hard sphere limit of a_2 with this effective restitution coefficient is known to reproduce the peak value of a_2 in Fig. 1 (Takada *et al.* 2017). Let us define the effective shear viscosity as

$$\eta_{\rm eff} = \frac{15}{2(1+e_{\rm eff})(13-e_{\rm eff})\sigma^2 g_2(\sigma)}\sqrt{\frac{mT}{\pi}}\left[1 + \frac{3(4-3e_{\rm eff})}{8(13-e_{\rm eff})}a_{2,\rm eff} + \frac{(7-4e_{\rm eff})}{32(13-e_{\rm eff})}a_{3,\rm eff}\right], \tag{5.3}$$

with $a_{2,\rm eff} \equiv a_2^{\rm (HC)}(e_{\rm eff})$ and $a_{3,\rm eff} \equiv a_3^{\rm (HC)}(e_{\rm eff})$. Figure 9 represents the temperature dependence of the effective shear viscosity (5.3). This simple effective theory (5.2) well reproduces the crossover temperature between two regimes.

We also consider the reason for the negativity of the coefficient μ in the intermediate temperature regime. Upon considering the relaxation dynamics of the hydrodynamic

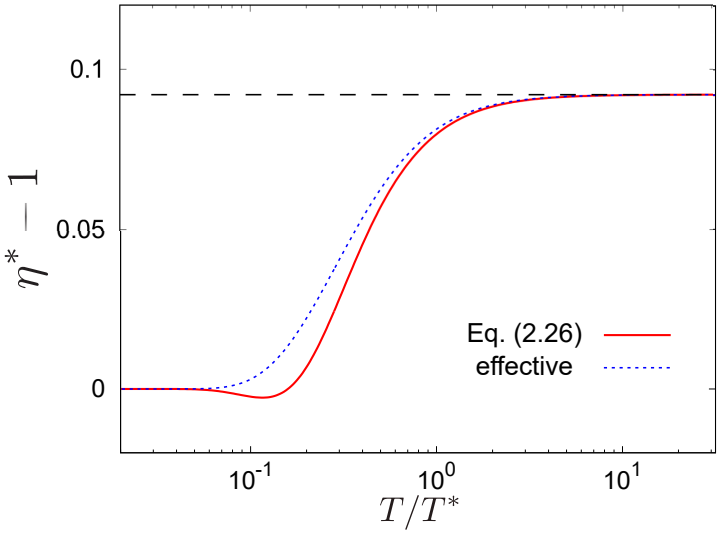

FIGURE 9. The temperature dependence of the shear viscosity obtained from the kinetic theory up to a_3 order (solid line) and that from the effective theory (dotted line). The dashed line is the shear viscosity of hard-sphere gases $\eta^{(\mathrm{HC})}(e^*)$.

fluxes by mean of a Grad expansion pertaining to granular gases, it was shown Sela & Goldhirsch (1998); Serero *et al.* (2009); Serero (2009) that the origin of the contribution to the heat flux proportional to the gradient of the density could be traced backed to the time dependence in granular gases of the microscopic time scale (the means free time). In the case of the heat flux, this dependence manifests itself through the emergence in the post-relaxation expression of the heat flux of a gradient of the cooling coefficient Serero *et al.* (2009); Serero (2009) (expressing the difference in the dynamics of the temperature on the sub-resolved scale), giving rise to a gradient of the density (see Serero (2009) and Serero *et al.* (2009) for a detailed derivation in the case of a monodisperse and bidisperse system of inelastic hard spheres, respectively). In the present case, this mechanism can yield a negative μ coefficient when combined with the particular form of the distribution function at hand, as detailed below. Note that this cannot be observed when we only use the Maxwell distribution function to determine the coefficient μ as shown in Fig. 10, which means that the origin of the negativeness comes from the deviation of the distribution function from the Gaussian. Let us consider two regions, one of which is slightly denser (system I) and the other is diluter (system II) with the same temperature around $T/T^* \simeq 0.1$. Although the distribution function is the same, the number of particles is different. Because the number of particles whose velocity is higher than v^* in system I is larger, the number of inelastic collisions increases, and the temperature of the former decays slightly faster than that of the latter. As a result, the temperature in system I is slightly smaller than that in system II ($T_{\mathrm{I}} \lesssim T_{\mathrm{II}}$), and this yields $a_2(T_{\mathrm{I}}) \gtrsim a_2(T_{\mathrm{II}})$. In addition, as our previous paper (Takada *et al.* 2017) reported, the population of the particles having $1 \lesssim v/v_{\mathrm{T}} \lesssim 2$ and $v/v_{\mathrm{T}} \gtrsim 2$ in the system I are higher and lower than those in the system II, respectively (in this case, $v_{\mathrm{T}} \simeq 0.3v^*$). Therefore, the heat flux goes from system II to system I, because the number of particles having higher velocities is larger in system II. This is the reason for the negative overshoot of μ in the intermediate temperature regime. It is noted that the transient behavior of the thermal conductivity is similarly explained.

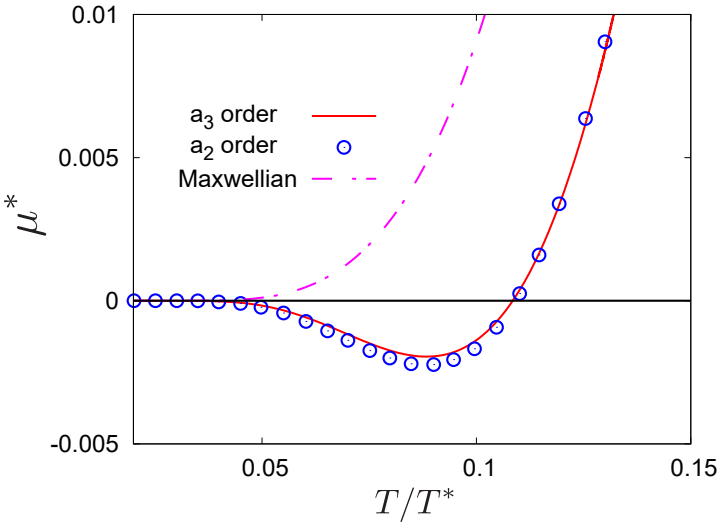

FIGURE 10. The temperature dependence of the coefficient μ obtained from the kinetic theory up to a_3 order (solid line), that up to a_2 order (open circles), and that determined from the Maxwell distribution function (dot-dashed line) for $e^* = 0.8$.

6. Conclusion

In this paper, we have derived the temperature dependence of the transport coefficients for charged granular gases. The negative overshoots of the transport coefficients appear because of the non-Gaussianity of the distribution function. Especially, we have found that the coefficient μ becomes negative in the intermediate temperature regime. We have also performed the linear stability analysis for the homogeneous cooling state, which shows the stability of the thermal and sound modes become reversal in the low-temperature regime, and this threshold is about $0.5T^*$. We have also performed the molecular dynamics simulation and we have obtained a consistent result with that from the kinetic theory.

Acknowledgments

Satoshi Takada wishes to express his sincere gratitude to the Yukawa Institute for Theoretical Physics for financial support towards his research visit at Friedrich-Alexander-Universität Erlangen-Nürnberg. Numerical computation in this work was partially carried out at the Yukawa Institute Computer Facility. We thank the Interdisciplinary Center for Nanostructured Films (IZNF), the Central Institute for Scientific Computing (ZISC), and the Interdisciplinary Center for Functional Particle Systems (FPS) at Friedrich-Alexander University Erlangen-Nürnberg.

Funding

This work was supported by Kompetenznetzwerk für wissenschaftliches Höchstleistungsrechnen in Bayern (KONWIHR) Satoshi Takada is partially supported by Scientific Grant-in-Aid of Japan Society for the Promotion of Science, KAKENHI (Grants Nos. 20K14428 and 21H01006).

Declaration of interests

The authors report no conflict of interest.

Author ORCID

Satoshi Takada https://orcid.org/0000-0002-2716-1846
Thorsten Pöschel https://orcid.org/0000-0001-5913-1070

Appendix A. Computation of the Sonine coefficients a_2 and a_3 from the Boltzmann equation

We expand the distribution function in Sonine polynomials up to third order, a_3, see Eq. (2.4). Then, we rewrite the expression of p-th moment of the collision integral in the form

$$\mu_p = -\frac{1}{2}\int d\boldsymbol{C}d\boldsymbol{c}_{12}d\hat{\boldsymbol{k}}\,\Theta(\boldsymbol{c}_{12}\cdot\hat{\boldsymbol{k}})\left|\boldsymbol{c}_{12}\cdot\hat{\boldsymbol{k}}\right|\phi(c_1)\phi(c_2) \times\left\{1+a_2\left[S_2(c_1^2)+S_2(c_2^2)\right]+a_3\left[S_3(c_1^2)+S_3(c_2^2)\right]\right\}\Delta(c_1^p+c_2^p), \quad (A\,1)$$

where we have neglected the terms proportional to a_2^2, a_3^2, and a_2a_3. The product of the dimensionless distribution function is then

$$\begin{aligned}
&1+a_2\left[S_2(c_1^2)+S_2(c_2^2)\right]+a_3\left[S_3(c_1^2)+S_3(c_2^2)\right]\\
&=1+a_2\left[C^4+\frac{1}{2}C^2c_{12}^2-5C^2+\frac{1}{16}c_{12}^4-\frac{5}{4}c_{12}^2+(\boldsymbol{C}\cdot\boldsymbol{c}_{12})^2+\frac{15}{4}\right]\\
&\quad+a_3\left[-\frac{1}{3}C^6-\frac{1}{4}C^4c_{12}^2+\frac{7}{2}C^4-\frac{1}{16}C^2c_{12}^4+\frac{7}{4}C^2c_{12}^2-C^2(\boldsymbol{C}\cdot\boldsymbol{c}_{12})^2-\frac{35}{4}C^2\right.\\
&\qquad\left.-\frac{1}{192}c_{12}^6+\frac{7}{32}c_{12}^4-\frac{1}{4}c_{12}^2(\boldsymbol{C}\cdot\boldsymbol{c}_{12})^2-\frac{35}{16}c_{12}^2+\frac{7}{2}(\boldsymbol{C}\cdot\boldsymbol{c}_{12})^2+\frac{35}{8}\right], \quad (A\,2)
\end{aligned}$$

and the terms $\Delta(c_1^p + c_2^p)$ for $p = 2$, 4, and 6 are, respectively, given by

$$\Delta(c_1^2 + c_2^2) = -\frac{1-e^2}{2}(\boldsymbol{c}_{12}\cdot\hat{\boldsymbol{k}})^2, \tag{A 3a}$$

$$\begin{aligned}\Delta(c_1^4 + c_2^4) = &-(1-e^2)C^2(\boldsymbol{c}_{12}\cdot\hat{\boldsymbol{k}})^2 - \frac{1}{4}(1-e^2)c_{12}^2(\boldsymbol{c}_{12}\cdot\hat{\boldsymbol{k}})^2\\ &- 4(1+e)(\boldsymbol{C}\cdot\boldsymbol{c}_{12})(\boldsymbol{C}\cdot\hat{\boldsymbol{k}})(\boldsymbol{c}_{12}\cdot\hat{\boldsymbol{k}})\\ &+ 2(1+e)^2(\boldsymbol{C}\cdot\hat{\boldsymbol{k}})^2(\boldsymbol{c}_{12}\cdot\hat{\boldsymbol{k}})^2 + \frac{(1-e^2)^2}{8}(\boldsymbol{c}_{12}\cdot\hat{\boldsymbol{k}})^4,\end{aligned} \tag{A 3b}$$

$$\begin{aligned}\Delta(c_1^6 + c_2^6) = &-\frac{3(1-e^2)}{2}C^4(\boldsymbol{c}_{12}\cdot\hat{\boldsymbol{k}})^2 - \frac{3(1-e^2)}{4}C^2c_{12}^2(\boldsymbol{c}_{12}\cdot\hat{\boldsymbol{k}})^2\\ &- 12(1+e)C^2(\boldsymbol{C}\cdot\boldsymbol{c}_{12})(\boldsymbol{C}\cdot\hat{\boldsymbol{k}})(\boldsymbol{c}_{12}\cdot\hat{\boldsymbol{k}}) + 6(1+e)^2C^2(\boldsymbol{C}\cdot\hat{\boldsymbol{k}})^2(\boldsymbol{c}_{12}\cdot\hat{\boldsymbol{k}})^2\\ &+ \frac{3(1-e^2)^2}{8}C^2(\boldsymbol{c}_{12}\cdot\hat{\boldsymbol{k}})^4 - \frac{3(1-e^2)}{32}c_{12}^4(\boldsymbol{c}_{12}\cdot\hat{\boldsymbol{k}})^2\\ &- 3(1+e)c_{12}^2(\boldsymbol{C}\cdot\boldsymbol{c}_{12})(\boldsymbol{C}\cdot\hat{\boldsymbol{k}})(\boldsymbol{c}_{12}\cdot\hat{\boldsymbol{k}}) + \frac{3(1+e)^2}{2}c_{12}^2(\boldsymbol{C}\cdot\hat{\boldsymbol{k}})^2(\boldsymbol{c}_{12}\cdot\hat{\boldsymbol{k}})^2\\ &+ \frac{3(1-e^2)^2}{32}c_{12}^2(\boldsymbol{c}_{12}\cdot\hat{\boldsymbol{k}})^4 - \frac{3(1-e^2)}{2}(\boldsymbol{C}\cdot\boldsymbol{c}_{12})^2(\boldsymbol{c}_{12}\cdot\hat{\boldsymbol{k}})^2\\ &+ 3(1+e)(1-e^2)(\boldsymbol{C}\cdot\boldsymbol{c}_{12})(\boldsymbol{C}\cdot\hat{\boldsymbol{k}})(\boldsymbol{c}_{12}\cdot\hat{\boldsymbol{k}})^3\\ &- \frac{3(1+e)^2(1-e^2)}{2}(\boldsymbol{C}\cdot\hat{\boldsymbol{k}})^2(\boldsymbol{c}_{12}\cdot\hat{\boldsymbol{k}})^4 - \frac{(1-e^2)^3}{32}(\boldsymbol{c}_{12}\cdot\hat{\boldsymbol{k}})^6.\end{aligned} \tag{A 3c}$$

Using Eqs. (A 2)–(A 3*c*), we can calculate μ_p for $p = 2$, 4, and 6 from Eq. (A 1) as

$$\mu_2 = \sqrt{2\pi}(S_1 + a_2S_2 + a_3S_3), \tag{A 4a}$$

$$\mu_4 = \sqrt{2\pi}(T_1 + a_2T_2 + a_3T_3), \tag{A 4b}$$

$$\mu_6 = \sqrt{2\pi}(D_1 + a_2D_2 + a_3D_3), \tag{A 4c}$$

with

$$S_1 = \frac{1}{2}\int_0^\infty dc_{12}\int_0^1 d(\cos\theta)(1-e^2)\cos^3\theta c_{12}^5\exp\left(-\frac{1}{2}c_{12}^2\right), \tag{A 5a}$$

$$S_2 = \frac{1}{32}\int_0^\infty dc_{12}\int_0^1 d(\cos\theta)(1-e^2)\cos^3\theta c_{12}^5(15 - 10c_{12}^2 + c_{12}^4)\exp\left(-\frac{1}{2}c_{12}^2\right), \tag{A 5b}$$

$$\begin{aligned}S_3 = \frac{1}{384}\int_0^\infty dc_{12}\int_0^1 &d(\cos\theta)(1-e^2)\cos^3\theta c_{12}^5\\ &\times(105 - 105c_{12}^2 + 21c_{12}^4 - c_{12}^6)\exp\left(-\frac{1}{2}c_{12}^2\right),\end{aligned} \tag{A 5c}$$

$$T_1 = \frac{1}{8}\int_0^\infty dc_{12}\int_0^1 d(\cos\theta)(1-e^2)\cos^3\theta c_{12}^5 \times\left[10+2c_{12}^2-(1-e^2)\cos^2\theta c_{12}^2\right]\exp\left(-\frac{1}{2}c_{12}^2\right), \tag{A 6a}$$

$$T_2 = \frac{1}{2}\int_0^\infty dc_{12}\int_0^1 d(\cos\theta)(1+e)\cos^3\theta c_{12}^5\exp\left(-\frac{1}{2}c_{12}^2\right) + \frac{1}{128}\int_0^\infty dc_{12}\int_0^1 d(\cos\theta)(1-e^2)\cos^3\theta c_{12}^5\exp\left(-\frac{1}{2}c_{12}^2\right) \times\left[2(-25-7c_{12}^2-5c_{12}^4+c_{12}^6)+\cos^2\theta c_{12}^2(17+10c_{12}^2-c_{12}^4) +e^2\cos^2\theta c_{12}^2(15-10c_{12}^2+c_{12}^4)\right], \tag{A 6b}$$

$$T_3 = \frac{1}{8}\int_0^\infty dc_{12}\int_0^1 d(\cos\theta)(1+e)\cos^3\theta(1-\cos^2\theta)c_{12}^7(7-c_{12}^2)\exp\left(-\frac{1}{2}c_{12}^2\right) + \frac{1}{1536}\int_0^\infty dc_{12}\int_0^1 d(\cos\theta)(1-e^2)\cos^3\theta c_{12}^5\exp\left(-\frac{1}{2}c_{12}^2\right) \times\left[2(-525+168c_{12}^2-54c_{12}^4+16c_{12}^6-c_{12}^8)+\cos^2\theta c_{12}^2(567+9c_{12}^2-21c_{12}^4+c_{12}^6) +e^2\cos^2\theta c_{12}^2(105-105c_{12}^2+21c_{12}^4-c_{12}^6)\right], \tag{A 6c}$$

$$D_1 = \frac{1}{32}\int_0^\infty dc_{12}\int_0^1 d(\cos\theta)(1-e^2)\cos^3\theta c_{12}^5\exp\left(-\frac{1}{2}c_{12}^2\right) \times\left[3(35+14c_{12}^2+c_{12}^4)-3(1-e^2)\cos^2\theta c_{12}^2(7+c_{12}^2)+(1-e^2)^2\cos^4\theta c_{12}^4\right], \tag{A 7a}$$

$$D_2 = \frac{3}{16}\int_0^\infty dc_{12}\int_0^1 d(\cos\theta)(1+e)\cos^3\theta c_{12}^7 \times\left[2-(1+e)\cos^2\theta\right]\left[7+c_{12}^2-(1-e^2)\cos^2\theta c_{12}^2\right]\exp\left(-\frac{1}{2}c_{12}^2\right) + \frac{1}{512}\int_0^\infty dc_{12}\int_0^1 d(\cos\theta)(1-e^2)\cos^3\theta c_{12}^5\exp\left(-\frac{1}{2}c_{12}^2\right) \times\left[3(-595-28c_{12}^2+14c_{12}^4+4c_{12}^6+c_{12}^8) +3(1-e^2)\cos^2\theta c_{12}^2(35+19c_{12}^2+3c_{12}^4-c_{12}^6) +(1-e^2)^2\cos^4\theta c_{12}^4(15-10c_{12}^2+c_{12}^4)\right], \tag{A 7b}$$

$$D_3 = \frac{3}{64}\int_0^\infty dc_{12}\int_0^1 d(\cos\theta)(1+e)\cos^3\theta c_{12}^7\exp\left(-\frac{1}{2}c_{12}^2\right) \times\left[2-(1+e)\cos^2\theta\right]\left[35-c_{12}^4-(1-e^2)\cos^2\theta c_{12}^2(7-c_{12}^2)\right] + \frac{1}{6144}\int_0^\infty dc_{12}\int_0^1 d(\cos\theta)(1-e^2)\cos^3\theta c_{12}^5\exp\left(-\frac{1}{2}c_{12}^2\right) \times\left[3(-5145+1575c_{12}^2+798c_{12}^4-74c_{12}^6+7c_{12}^8-c_{12}^{10}) +3(1-e^2)\cos^2\theta c_{12}^2(735-126c_{12}^2+24c_{12}^4-14c_{12}^6+c_{12}^8) +(1-e^2)^2\cos^4\theta c_{12}^4(105-105c_{12}^2+21c_{12}^4-c_{12}^6)\right]. \tag{A 7c}$$

Here, we use the relations between the moments μ_p of different order,

$$\mu_4 = 5\mu_2(1+2a_2), \tag{A 8a}$$

$$\mu_6 = \frac{105}{4}\mu_2(1+3a_2-a_3). \tag{A 8b}$$

Substituting Eqs. (A 4) into Eqs. (A 8), we obtain

$$(5S_1+5S_2-T_2)a_2+(5S_3-T_3)a_3 = T_1-5S_1, \tag{A 9a}$$

$$\left(\frac{315}{4}S_1+\frac{105}{4}S_2-D_2\right)a_2+\left(-\frac{105}{4}S_1+\frac{105}{4}S_3-D_3\right)a_3 = D_1-\frac{105}{4}S_1. \tag{A 9b}$$

Using Eqs. (A 9), we obtain the coefficients a_2 and a_3 in the form given by Eq. (2.9).

In the discontinuous limit, $\beta v^* \to \infty$, Eqs. (A 5a)–(A 7c) read

$$S_1^{(\infty)} = \left(1-e^{*2}\right)(1+x)e^{-x}, \tag{A 10a}$$

$$S_2^{(\infty)} = \frac{3}{16}\left(1-e^{*2}\right)\left(1+x+\frac{x^2}{3}\right)e^{-x}, \tag{A 10b}$$

$$S_3^{(\infty)} = \frac{1}{64}\left(1-e^{*2}\right)\left(1+x-2x^2+\frac{28}{3}x^3-\frac{8}{3}x^4\right)e^{-x}, \tag{A 10c}$$

$$T_1^{(\infty)} = \left(1-e^{*2}\right)\left[\frac{9}{2}\left(1+x+\frac{x^2}{9}\right)+e^{*2}\left(1+x+\frac{x^2}{2}\right)\right]e^{-x}, \tag{A 11a}$$

$$\begin{aligned} T_2^{(\infty)} = {} & \frac{3}{32}\left(1-e^{*2}\right)\left[69\left(1+x+\frac{119x^2}{207}+\frac{32x^3}{207}+\frac{4x^4}{207}\right)\right. \\ & \left.+10e^{*2}\left(1+x+\frac{x^2}{2}+\frac{2x^3}{15}+\frac{2x^4}{15}\right)\right]e^{-x} \\ & -2\left(1-e^*\right)(1+x)e^{-x}+4, \end{aligned} \tag{A 11b}$$

$$\begin{aligned} T_3^{(\infty)} = {} & -\frac{1}{128}(1-e^{*2})\left[117\left(1+x+\frac{19}{117}x^2+\frac{10}{13}x^3+\frac{4}{39}x^4+\frac{8}{351}x^5\right)\right. \\ & \left.+10e^{*2}\left(1+x+\frac{x^2}{2}+\frac{x^3}{3}-\frac{2x^4}{3}+\frac{4x^5}{15}\right)\right]e^{-x} \\ & +\frac{1}{2}(1-e^*)(1+x+2x^2)e^{-x}-1, \end{aligned} \tag{A 11c}$$

$$\begin{aligned} D_1^{(\infty)} = {} & \frac{3}{16}(1-e^{*2})\left[115\left(1+x+\frac{22x^2}{115}+\frac{4x^3}{345}\right)+44e^{*2}\left(1+x+\frac{x^2}{2}+\frac{x^3}{33}\right)\right. \\ & \left.+8e^{*4}\left(1+x+\frac{x^2}{2}+\frac{x^3}{6}\right)\right]e^{-x}, \end{aligned} \tag{A 12a}$$

$$\begin{aligned} D_2^{(\infty)} = {} & \frac{3}{256}(1-e^{*2})\left[5737\left(1+x+\frac{2850x^2}{5737}+\frac{2120x^3}{17211}+\frac{248x^4}{17211}+\frac{16x^5}{17211}\right)\right. \\ & +1572e^{*2}\left(1+x+\frac{x^2}{2}+\frac{221x^3}{1179}+\frac{62x^4}{1179}+\frac{4x^5}{1179}\right) \\ & \left.+280e^{*4}\left(1+x+\frac{x^2}{2}+\frac{x^3}{6}+\frac{4x^4}{105}+\frac{2x^5}{105}\right)\right]e^{-x} \\ & +\frac{3}{2}(1+e^*)\left[20\left(1+x+\frac{9x^2}{40}\right)-9e^*\left(1+x+\frac{x^2}{2}\right)+10e^{*2}\left(1+x+\frac{x^2}{2}+\frac{x^3}{10}\right)\right. \end{aligned}$$

$$-6e^{*3}\left(1+x+\frac{x^2}{2}+\frac{x^3}{6}\right)\Bigg]e^{-x}$$

$$-45\left(1+x+\frac{2x^2}{15}\right)e^{-x}+45, \tag{A 12b}$$

$$D_3^{(\infty)}=-\frac{3}{1024}(1-e^{*2})\left[9161\left(1+x+\frac{4528x^2}{9161}+\frac{2132x^3}{9161}+\frac{1640x^4}{27483}+\frac{128x^5}{27483}+\frac{32x^6}{27483}\right)\right.$$
$$+1636e^{*2}\left(1+x+\frac{x^2}{2}+\frac{140x^3}{1227}+\frac{76x^4}{1227}+\frac{32x^5}{1227}+\frac{8x^6}{3681}\right)$$
$$\left.+280e^{*4}\left(1+x+\frac{x^2}{2}+\frac{x^3}{6}+\frac{x^4}{21}-\frac{2x^5}{105}+\frac{4x^6}{315}\right)\right]e^{-x}$$
$$-\frac{9}{8}(1+e^*)\left[20\left(1+x+\frac{71x^2}{120}+\frac{3x^3}{20}\right)-9e^*\left(1+x+\frac{x^2}{2}+\frac{x^3}{3}\right)\right.$$
$$+10e^{*2}\left(1+x+\frac{x^2}{2}+\frac{7x^3}{30}+\frac{x^4}{15}\right)$$
$$\left.-6e^{*3}\left(1+x+\frac{x^2}{2}+\frac{x^3}{6}+\frac{x^4}{9}\right)\right]e^{-x}$$
$$+\frac{135}{4}\left(1+x+\frac{28x^2}{45}+\frac{4x^3}{45}\right)e^{-x}-\frac{135}{4}. \tag{A 12c}$$

It can be shown that in the limit $x\to 0$, the above expressions are identical to the corresponding expressions for hard-sphere gas (Brilliantov & Pöschel 2006; Santos & Montanero 2009; Chamorro *et al.* 2013). Using Eq. (A 9), we can also obtain explicit expressions for a_2 and a_3. These expressions are rather cumbersome and not shown here.

Appendix B. Calculation of Ω_η^e and Ω_κ^e given by Eqs. (2.11) and (2.14)

Using the definition of $\widetilde{D}_{\alpha\beta}(\boldsymbol{c})$, Eq. (2.12), we obtain

$$
\begin{aligned}
&\widetilde{D}_{\alpha\beta}(\boldsymbol{c}_2)\Delta[\widetilde{D}_{\alpha\beta}(\boldsymbol{c}_1)+\widetilde{D}_{\alpha\beta}(\boldsymbol{c}_2)]\\
&=\left(c_{2i}c_{2j}-\frac{1}{3}\delta_{ij}c_2^2\right)\left[c'_{1i}c'_{1j}+c'_{2i}c'_{2j}-c_{1i}c_{1j}-c_{2i}c_{2j}-\frac{1}{3}\delta_{ij}\left(c_1'^2+c_2'^2-c_1^2-c_2^2\right)\right]\\
&=\frac{1-e^2}{6}C^2(\boldsymbol{c}_{12}\cdot\hat{\boldsymbol{k}})^2+\frac{1+e}{2}c_{12}^2(\boldsymbol{C}\cdot\hat{\boldsymbol{k}})(\boldsymbol{c}_{12}\cdot\hat{\boldsymbol{k}})-\frac{(1+e)(5+e)}{24}c_{12}^2(\boldsymbol{c}_{12}\cdot\hat{\boldsymbol{k}})^2\\
&\quad-(1+e)(\boldsymbol{C}\cdot\boldsymbol{c}_{12})(\boldsymbol{C}\cdot\hat{\boldsymbol{k}})(\boldsymbol{c}_{12}\cdot\hat{\boldsymbol{k}})+\frac{(1+e)(2+e)}{6}(\boldsymbol{C}\cdot\boldsymbol{c}_{12})(\boldsymbol{c}_{12}\cdot\hat{\boldsymbol{k}})^2\\
&\quad+\frac{(1+e)^2}{2}(\boldsymbol{C}\cdot\hat{\boldsymbol{k}})^2(\boldsymbol{c}_{12}\cdot\hat{\boldsymbol{k}})^2-\frac{(1+e)^2}{2}(\boldsymbol{C}\cdot\hat{\boldsymbol{k}})(\boldsymbol{c}_{12}\cdot\hat{\boldsymbol{k}})^3+\frac{(1+e)^2}{8}(\boldsymbol{c}_{12}\cdot\hat{\boldsymbol{k}})^4. \qquad \text{(B 1)}
\end{aligned}
$$

We also use the expressions of the Sonine expansion as

$$
\begin{aligned}
&1+a_2S_2(c_1)^2+a_3S_3(c_1^2)\\
&=1+a_2\left[\frac{1}{2}C^4+\frac{1}{4}C^2c_{12}^2+C^2(\boldsymbol{C}\cdot\boldsymbol{c}_{12})-\frac{5}{2}C^2+\frac{1}{32}c_{12}^4\right.\\
&\qquad\left.+\frac{1}{4}c_{12}^2(\boldsymbol{C}\cdot\boldsymbol{c}_{12})-\frac{5}{8}c_{12}^2+\frac{1}{2}(\boldsymbol{C}\cdot\boldsymbol{c}_{12})^2-\frac{5}{2}(\boldsymbol{C}\cdot\boldsymbol{c}_{12})+\frac{15}{8}\right]\\
&\quad+a_3\left[-\frac{1}{6}C^6-\frac{1}{8}C^4c_{12}^2-\frac{1}{2}C^4(\boldsymbol{C}\cdot\boldsymbol{c}_{12})+\frac{7}{4}C^4-\frac{1}{32}C^2c_{12}^4-\frac{1}{4}C^2c_{12}^2(\boldsymbol{C}\cdot\boldsymbol{c}_{12})\right.\\
&\qquad+\frac{7}{8}C^2c_{12}^2-\frac{1}{2}C^2(\boldsymbol{C}\cdot\boldsymbol{c}_{12})^2+\frac{7}{2}C^2(\boldsymbol{C}\cdot\boldsymbol{c}_{12})-\frac{35}{8}C^2-\frac{1}{384}c_{12}^6\\
&\qquad-\frac{1}{32}c_{12}^4(\boldsymbol{C}\cdot\boldsymbol{c}_{12})+\frac{7}{64}c_{12}^4-\frac{1}{8}c_{12}^2(\boldsymbol{C}\cdot\boldsymbol{c}_{12})^2+\frac{7}{8}c_{12}^2(\boldsymbol{C}\cdot\boldsymbol{c}_{12})\\
&\qquad\left.-\frac{35}{32}c_{12}^2-\frac{1}{6}(\boldsymbol{C}\cdot\boldsymbol{c}_{12})^3+\frac{7}{4}(\boldsymbol{C}\cdot\boldsymbol{c}_{12})^2-\frac{35}{8}(\boldsymbol{C}\cdot\boldsymbol{c}_{12})+\frac{35}{16}\right]. \qquad \text{(B 2)}
\end{aligned}
$$

Substituting Eqs. (B 1) and (B 2) into Eq. (2.11), we obtain

$$
\Omega_\eta^e\equiv\sqrt{2\pi}\left(\omega_{\eta,1}^e+a_2\omega_{\eta,2}^e+a_3\omega_{\eta,3}^e\right), \qquad \text{(B 3)}
$$

with

$$
\omega_{\eta,1}^e=-\frac{1}{12}\int_0^\infty dc_{12}\int_0^1 d(\cos\theta)(1+e)\left[5+e-3(1+e)\cos^2\theta\right]\cos^3\theta c_{12}^7\exp\left(-\frac{1}{2}c_{12}^2\right), \qquad \text{(B 4}a\text{)}
$$

$$
\begin{aligned}
\omega_{\eta,2}^e=&-\frac{1}{384}\int_0^\infty dc_{12}\int_0^1 d(\cos\theta)(1+e)\left[5+e-3(1+e)\cos^2\theta\right]\\
&\times\cos^3\theta c_{12}^7(63-18c_{12}^2+c_{12}^4)\exp\left(-\frac{1}{2}c_{12}^2\right), \qquad \text{(B 4}b\text{)}
\end{aligned}
$$

$$
\begin{aligned}
\omega_{\eta,3}^e=&-\frac{1}{4608}\int_0^\infty dc_{12}\int_0^1 d(\cos\theta)(1+e)\left[5+e-3(1+e)\cos^2\theta\right]\\
&\times\cos^3\theta c_{12}^7(693-297c_{12}^2+33c_{12}^4-c_{12}^6)\exp\left(-\frac{1}{2}c_{12}^2\right). \qquad \text{(B 4}c\text{)}
\end{aligned}
$$

For $\beta v^* \to \infty$, these quantities reduce to

$$\omega_{\eta,1}^{e(\infty)} = -4 + (1-e^*)\left[(1-e^*)(1+x) - \frac{2}{3}(1+e^*)x^2\right] e^{-x} \tag{B 5a}$$

$$\omega_{\eta,2}^{e(\infty)} = \frac{1}{8} - \frac{1}{32}(1-e^*)\left[(1-e^*)(1+x) + 6(9+e^*)x^2 - 4(13+7e^*)x^3\right. \tag{B 5b}$$

$$\left. +8(1+e^*)x^4\right] e^{-x}, \tag{B 5c}$$

$$\omega_{\eta,3}^{e(\infty)} = \frac{1}{32} - \frac{1}{128}(1-e^*)\left[(1-e^*)(1+x) + \frac{4}{3}(31+4e^*)x^2 - \frac{8}{3}(24+11e^*)x^3\right.$$

$$\left. +\frac{16}{3}(4+3e^*)x^4 - \frac{16}{9}(1+e^*)x^5\right] e^{-x}. \tag{B 5d}$$

In a similar way, we derive Ω_κ^e defined by Eq. (2.14). Using the definition of $\widetilde{\boldsymbol{S}}(\boldsymbol{c})$, Eq. (2.15), we write

$$\begin{aligned}
&\tilde{\boldsymbol{S}}(\boldsymbol{c}_2)\cdot\Delta\left[\tilde{\boldsymbol{S}}(\boldsymbol{c}_1)+\tilde{\boldsymbol{S}}(\boldsymbol{c}_2)\right]\\
&= \left(c_2^2 - \frac{5}{2}\right)\left[(\boldsymbol{c}_1'\cdot\boldsymbol{c}_2)c_1'^2 + (\boldsymbol{c}_2'\cdot\boldsymbol{c}_2)c_2'^2 - (\boldsymbol{c}_1\cdot\boldsymbol{c}_2)c_1^2 - (\boldsymbol{c}_2\cdot\boldsymbol{c}_2)c_2^2\right]\\
&= -\frac{1-e^2}{2}C^4(\boldsymbol{c}_{12}\cdot\hat{\boldsymbol{k}})^2 + \frac{1+e}{2}C^2c_{12}^2(\boldsymbol{C}\cdot\hat{\boldsymbol{k}})(\boldsymbol{c}_{12}\cdot\hat{\boldsymbol{k}}) - \frac{1-e^2}{8}C^2c_{12}^2(\boldsymbol{c}_{12}\cdot\hat{\boldsymbol{k}})^2\\
&\quad - 2(1+e)C^2(\boldsymbol{C}\cdot\boldsymbol{c}_{12})(\boldsymbol{C}\cdot\hat{\boldsymbol{k}})(\boldsymbol{c}_{12}\cdot\hat{\boldsymbol{k}}) + \frac{(1+e)(5-3e)}{4}C^2(\boldsymbol{C}_{12}\cdot\boldsymbol{c}_{12})(\boldsymbol{c}_{12}\cdot\hat{\boldsymbol{k}})^2\\
&\quad + (1+e)^2C^2(\boldsymbol{C}\cdot\hat{\boldsymbol{k}})^2(\boldsymbol{c}_{12}\cdot\hat{\boldsymbol{k}})^2 - \frac{(1+e)^2}{2}C^2(\boldsymbol{C}\cdot\hat{\boldsymbol{k}})(\boldsymbol{c}_{12}\cdot\hat{\boldsymbol{k}})^3\\
&\quad + \frac{5(1-e^2)}{4}C^2(\boldsymbol{c}_{12}\cdot\hat{\boldsymbol{k}})^2 + \frac{1+e}{8}c_{12}^4(\boldsymbol{C}\cdot\hat{\boldsymbol{k}})(\boldsymbol{c}_{12}\cdot\hat{\boldsymbol{k}}) - (1+e)c_{12}^2(\boldsymbol{C}\cdot\boldsymbol{c}_{12})(\boldsymbol{C}\cdot\hat{\boldsymbol{k}})(\boldsymbol{c}_{12}\cdot\hat{\boldsymbol{k}})\\
&\quad + \frac{(1+e)(3-e)}{16}c_{12}^2(\boldsymbol{C}\cdot\boldsymbol{c}_{12})(\boldsymbol{c}_{12}\cdot\hat{\boldsymbol{k}})^2 + \frac{(1+e)^2}{4}c_{12}^2(\boldsymbol{C}\cdot\hat{\boldsymbol{k}})^2(\boldsymbol{c}_{12}\cdot\hat{\boldsymbol{k}})^2\\
&\quad - \frac{(1+e)^2}{8}c_{12}^2(\boldsymbol{C}\cdot\hat{\boldsymbol{k}})(\boldsymbol{c}_{12}\cdot\hat{\boldsymbol{k}})^3 - \frac{5(1+e)}{4}c_{12}^2(\boldsymbol{C}\cdot\hat{\boldsymbol{k}})(\boldsymbol{c}_{12}\cdot\hat{\boldsymbol{k}})\\
&\quad + 2(1+e)(\boldsymbol{C}\cdot\boldsymbol{c}_{12})^2(\boldsymbol{C}\cdot\hat{\boldsymbol{k}})(\boldsymbol{c}_{12}\cdot\hat{\boldsymbol{k}}) - \frac{(1+e)(3-e)}{4}(\boldsymbol{C}\cdot\boldsymbol{c}_{12})^2(\boldsymbol{c}_{12}\cdot\hat{\boldsymbol{k}})^2\\
&\quad - (1+e)^2(\boldsymbol{C}\cdot\boldsymbol{c}_{12})(\boldsymbol{C}\cdot\hat{\boldsymbol{k}})^2(\boldsymbol{c}_{12}\cdot\hat{\boldsymbol{k}})^2 + \frac{(1+e)^2}{2}(\boldsymbol{C}\cdot\boldsymbol{c}_{12})(\boldsymbol{C}\cdot\hat{\boldsymbol{k}})(\boldsymbol{c}_{12}\cdot\hat{\boldsymbol{k}})^3\\
&\quad + 5(1+e)(\boldsymbol{C}\cdot\boldsymbol{c}_{12})(\boldsymbol{C}\cdot\hat{\boldsymbol{k}})(\boldsymbol{c}_{12}\cdot\hat{\boldsymbol{k}}) - \frac{5(1+e)(3-e)}{8}(\boldsymbol{C}\cdot\boldsymbol{c}_{12})(\boldsymbol{c}_{12}\cdot\hat{\boldsymbol{k}})^2\\
&\quad - \frac{5(1+e)^2}{2}(\boldsymbol{C}\cdot\hat{\boldsymbol{k}})^2(\boldsymbol{c}_{12}\cdot\hat{\boldsymbol{k}})^2 + \frac{5(1+e)^2}{4}(\boldsymbol{C}\cdot\hat{\boldsymbol{k}})(\boldsymbol{c}_{12}\cdot\hat{\boldsymbol{k}})^3.
\end{aligned} \tag{B 6}$$

With Eqs. (B 2), (B 6), and (2.14), we obtain

$$\Omega_\kappa^e \equiv \sqrt{2\pi}\left(\omega_{\kappa,1}^e + a_2\omega_{\kappa,2}^e + a_3\omega_{\kappa,3}^e\right), \tag{B 7}$$

with

$$\omega^e_{\kappa,1} = \frac{1}{16}\int_0^\infty dc_{12}\int_0^1 d(\cos\theta)(1+e)\cos^3\theta c_{12}^5 \times\left[25(1-e)-(15-7e)c_{12}^2+4(1+e)\cos^2\theta c_{12}^2\right]\exp\left(-\frac{1}{2}c_{12}^2\right), \tag{B 8a}$$

$$\omega^e_{\kappa,2} = \frac{1}{512}\int_0^\infty dc_{12}\int_0^1 d(\cos\theta)(1+e)\cos^3\theta c_{12}^5\exp\left(-\frac{1}{2}c_{12}^2\right) \times\left[175(1-e)+7(35+37e)c_{12}^2-(85+59e)c_{12}^4+(5+3e)c_{12}^6 -4(1+e)(63-18c_{12}^2+c_{12}^4)\cos^2\theta c_{12}^2\right], \tag{B 8b}$$

$$\omega^e_{\kappa,3} = \frac{1}{6144}\int_0^\infty dc_{12}\int_0^1 d(\cos\theta)(1+e)\cos^3\theta c_{12}^5\exp\left(-\frac{1}{2}c_{12}^2\right) \times\left[-1575(1-e)+252(45-e)c_{12}^2-54(85+3e)c_{12}^4+4(125+7e)c_{12}^6 -(15+e)c_{12}^8-8(1+e)(693-297c_{12}^2+33c_{12}^4-c_{12}^6)\cos^2\theta c_{12}^2\right]. \tag{B 8c}$$

For $\beta v^* \to \infty$, these quantities reduce to

$$\omega^{e(\infty)}_{\kappa,1} = -4-\frac{1}{8}(1-e^*)\left[(17+33e^*)(1+x)+22(1+e^*)x^2\right]e^{-x}, \tag{B 9a}$$

$$\omega^{e(\infty)}_{\kappa,2} = -\frac{1}{8}+\frac{1}{256}(1-e^*) \times\left[(13-3e^*)(1+x)+2(67+3e^*)x^2-4(23+7e^*)x^3+8(1+e^*)x^4\right]e^{-x}, \tag{B 9b}$$

$$\omega^{e(\infty)}_{\kappa,3} = -\frac{1}{16}+\frac{1}{1024}(1-e^*)\left[(11-21e^*)(1+x)+16(43+7e^*)x^2 -\frac{8}{3}(439+231e^*)x^3+\frac{16}{3}(79+63e^*)x^4-\frac{112}{3}(1+e^*)x^5\right]e^{-x}. \tag{B 9c}$$

Appendix C. Numerical solution of the transport coefficients

Here, we provide some details of the numerical solution of the differential equations for the transport coefficients. Consider first the shear viscosity. Special care is in order since the corresponding differential equation (2.25) is singular due to the fact that the coefficient of $\partial\eta^*/\partial x$ vanishes in both limits $x \to 0$ and $x \to \infty$.

Also the proper boundary conditions of this equation requires attention: In the high-temperature limit, all particles are expected to collide inelastically with one another, while in the limit of low temperature elastic interactions dominate. Thus, in the limit of high temperature, we expect the shear viscosity of a granular gas with coefficient of restitution e^*. For low temperature we expect the shear viscosity of an elastic hard-sphere gas, that is coefficient of restitution 1. The proper boundary condition reads, therefore,

$$\lim_{x\to 0}\eta^* = \frac{\eta^{(\mathrm{HC})}(e^*)}{\eta^{(\mathrm{HC})}(1)}, \tag{C 1}$$

with

$$\eta^{(\mathrm{HC})}(e^*) \equiv \frac{15}{2(1+e^*)(13-e^*)\sigma^2 g_2(\sigma)}\sqrt{\frac{mT}{\pi}} \times \left[1+\frac{3(4-3e^*)}{8(13-e^*)}a_2^{(\mathrm{HC})}(e^*)+\frac{(7-4e^*)}{32(13-e^*)}a_3^{(\mathrm{HC})}(e^*)\right], \quad (\mathrm{C}\,2)$$

(see also (Brilliantov & Pöschel 2006; Chamorro *et al.* 2013)).

For the numerical solution of Eq. (2.25), we decompose the interval $x \in (0,\infty)$ into three intervals, (i) $x \in (0, e^{-1})$, (ii) $x \in [e^{-1}, e^{e/2})$, and (iii) $x \in [e^{e/2}, \infty)$.

In case (i), we introduce the new variable $y_1 \equiv \log x$ with $y_1 \in (-\infty, -1)$. Equation (2.25) reads then

$$10\mu_2^e e^{-e^{y_1}}\frac{\partial \eta^*}{\partial y_1} - (5\mu_2 + 6\Omega_\eta)\,\eta^* = 24\sqrt{2\pi} \quad \text{with} \quad \mu_2^e \equiv \mu_2 e^x \quad (\mathrm{C}\,3)$$

and the correspondingly boundary condition

$$\lim_{y_1\to-\infty}\eta^* = \frac{\eta^{(\mathrm{HC})}(e^*)}{\eta^{(\mathrm{HC})}(1)}\,. \quad (\mathrm{C}\,4)$$

In the next region (ii), we can directly solve Eq. (2.25) since the coefficient of the derivative of η^* in Eq. (2.25) is not small. The corresponding boundary condition reads

$$\lim_{x\to e^{-1}+0}\eta^* = \lim_{x\to e^{-1}-0}\eta^*, \quad (\mathrm{C}\,5)$$

where the right hand side of this equation should be evaluated in terms of Eq. (C 3). Finally, when considering region (iii), we introduce $y_2 \equiv e^x$ with $y_2 \in (e/2, \infty)$. Equation (2.25) reads then

$$10\mu_2^e \log y_2 \frac{\partial \eta^*}{\partial y_2} - (5\mu_2 + 6\Omega_\eta)\,\eta^* = 24\sqrt{2\pi}. \quad (\mathrm{C}\,6)$$

In a similar way we solve numerically the differential equations (2.29) for the thermal conductivity and (2.30) for the coefficient μ. The corresponding boundary conditions read

$$\lim_{x\to 0}\kappa^* = \frac{\kappa^{(\mathrm{HC})}(e^*)}{\sqrt{T}}, \quad \lim_{x\to 0}\mu^* = \frac{\mu^{(\mathrm{HC})}(e^*)}{\sqrt{T^{3/2}}}, \quad (\mathrm{C}\,7)$$

with

$$\kappa^{(\mathrm{HC})}(e^*) \equiv \frac{75}{2(1+e^*)(9+7e^*)\sigma^2 g_2(\sigma)}\sqrt{\frac{T}{\pi m}} \times \left[1+\frac{797+211e^*}{32(9+7e^*)}a_2^{(\mathrm{HC})}(e^*)+\frac{27-59e^*}{128(9+7e^*)}a_3^{(\mathrm{HC})}(e^*)\right], \quad (\mathrm{C}\,8)$$

$$\mu^{(\mathrm{HC})}(e^*) \equiv \frac{750(1-e^*)}{(1+e^*)(9+7e^*)(19-3e^*)n\sigma^2 g_2(\sigma)}\sqrt{\frac{T^3}{\pi m}} \times \left[1+\frac{50201-30971e^*-7253e^{*2}+4407e^{*3}}{80(1-e^*)(19-3e^*)(9+7e^*)}a_2^{(\mathrm{HC})}(e^*) + \frac{459-646e^*-69e^{*2}}{64(19-3e^*)(9+7e^*)}a_3^{(\mathrm{HC})}(e^*)\right], \quad (\mathrm{C}\,9)$$

(see also Refs. (Brilliantov & Pöschel 2006; Chamorro *et al.* 2013)).

REFERENCES

Brey, J. J. & Cubero, D. 2001 Hydrodynamic transport coefficients of granular gases. In *Granular Gases*, Granular gases edn. (ed. T. Pöschel & S. Luding), *Lecture Notes in Physics*, vol. 564, pp. 59–78. Springer.

Brey, J. J., Dufty, J. W., Kim, C. S. & Santos, A. 1998 Hydrodynamics for granular flow at low density. *Phys. Rev. E* **58**, 4638–4653.

Brey, J. J. & Ruiz-Montero, M. 2004 Simulation study of the green-kubo relations for dilute granular gases. *Phys. Rev. E* **70**, 051301.

Brey, J. J., Ruiz-Montero, M. J., Maynar, P. & García de Soria, M. 2005 Hydrodynamic modes, green-kubo relations, and velocity correlations in dilute granular gases. *J. Phys.: Condens. Matter* **17**, S2489.

Brilliantov, N. B., Salueña, C., Pöschel, T. & Schwager, T. 2004 Clustering and vortex formation as a transient process in granular gases. *Phys. Rev. Lett.* **93**, 134301.

Brilliantov, N. V. & Pöschel, T. 2000 Deviation from Maxwell distribution in granular gases with constant restitution coefficient. *Phys. Rev. E* **61**, 2809.

Brilliantov, N. V. & Pöschel, T. 2006 Breakdown of the Sonine expansion for the velocity distribution of granular gases. *Europhys. Lett.* **74**, 424–430.

Brilliantov, N. V., Spahn, F., Hertzsch, J.-M. & Pöschel, T. 1996 Model for collisions in granular gases. *Phys. Rev. E* **53**, 5382.

Brilliantov, N. V. & T. Pöschel, T. 2004 *Kinetic Theory of Granular Gases*. Oxford University Press.

Chamorro, M. G., Reyes, F. V. & Garzó, V. 2013 Homogeneous steady states in a granular fluid driven by a stochastic bath with friction. *J. Stat. Mech* p. P07013.

Dufty, J. W. & Brey, J. 2002 Green-Kubo expressions for a granular gas. *J. Stat. Phys* **109**, 433–448.

Esipov, S. E. & Pöschel, T. 1997 The granular phase diagram. *J. Stat. Phys.* **86**, 1385.

Garzó, V. 2019 *Granular Gaseous Flows: A Kinetic Theory Approach to Granular Gaseous Flows*. Berlin: Springer.

Genareau, K., Wardman, J. B., Wilson, T. M., McNutt, S. R. & Izbekov, P. 2015 Lightning-induced volcanic spherules. *Geology* **43**, 319–322.

Goldhirsch, I. 2003 Rapid granular flows. *Annual Review of Fluid Mechanics* **35**, 267–293.

Goldhirsch, I., Noskowicz, S. H. & Bar-Lev, O. 2003 The homogeneous cooling state revisited. In Pöschel & Brilliantov (2003), pp. 37–63.

Goldhirsch, I. & Zanetti, G. 1993 Clustering instability in dissipative gases. *Phys. Rev. Lett.* **70**, 1619.

Goldshtein, A. & Shapiro, M. 1995 Mechanics of collisional motion of granular materials. Part 1: General hydrodynamic equations. *J. Fluid Mech* **282**, 75.

Haff, P. K. 1983 Grain flow as a fluid-mechanical phenomenon. *J. Fluid Mech* **134**, 401–430.

Jungmann, F., Steinpilz, T., Teiser, J. & Wurm, G. 2018 Sticking and restitution in collisions of charged sub-mm dielectric grains. *J. Phys. Commun.* **2**, 095009.

Kanazawa, S., Ohkubo, T., Nomoto, Y. & Adachi, T. 1995 Electrification of a pipe wall during powder transport. *J. Electrostat.* **35**, 47–54.

Kolehmainen, J., Ozel, A., Boyce, C. M. & Sundaresan, S. 2016 A hybrid approach to computing electrostatic forces in fluidized beds of charged particles. *AIChE J.* **62**, 2282–2295.

Kumar, D., Sane, A., Gohil, S., Bandaru, P. R., Bhattacharya, S. & Ghosh, S. 2014 Spreading of triboelectrically charged granular matter. *Sci. Reports* **4**, 5275.

Lacks, Daniel J. & Shinbrot, Troy 2019 Long-standing and unresolved issues in triboelectric charging. *Nature Reviews Chemistry* **3**, 465–476.

Laurentie, J. C., Traoré, P. & Dascalescu, L. 2013 Discrete element modeling of triboelectric charging of insulating materials in vibrated granular beds. *J. Electrostat.* **71**, 951–957.

Lee, V., Waitukaitis, S. R., Miskin, M. Z. & Jaeger, H. M. 2015 Direct observation of particle interactions and clustering in charged granular streams. *Nature Phys.* **11**, 733–737.

Muranushi, T. 2010 Dust-dust collisional charging and lightning in protoplanetary discs. *Mon. Not. R. Astron. Soc.* **401**, 2641–2664.

van Noije, T. P. C. & Ernst, M. H. 1998 Velocity distributions in homogeneous granular fluids: the free and the heated case. *Granular Matter* **1**, 57.

Pan, Shuaihang & Zhang, Zhinan 2019 Fundamental theories and basic principles of triboelectric effect: A review. *Friction* **7**, 2–17.

Pöschel, T. & Brilliantov, N. V., ed. 2003 *Granular Gas Dynamics*, *Lecture Notes in Physics*, vol. 624. Springer.

Pöschel, T., Brilliantov, N. V. & Schwager, T. 2003 Long-time behavior of granular gases with impact-velocity dependent coefficient of restitution. *Physica A* **325**, 274–283.

Puglisi, A. 2015 *Transport and Fluctuations in Granular Fluids*, *Springer Briefs in Physics*, vol. 34. Springer.

Santos, A., Garzó, V. & Dufty, J. W. 2004 Inherent rheology of a granular fluid in uniform shear flow. *Phys. Rev. E* **69**, 061303.

Santos, A. & Montanero, J. M. 2009 The second and third Sonine coefficients of a freely cooling granular gas revisited. *Granul. Matter* **11**, 157–168.

Scheffler, T. & Wolf, D. E. 2002 Collision rates in charged granular gases. *Granular Matter* **4**, 103–113.

Schwager, T. & Pöschel, T. 2008 Coefficient of restitution for viscoelastic spheres: The effect of delayed recovery. *Phys. Rev. E* **78**, 051304.

Sela, N. & Goldhirsch, I. 1998 Hydrodynamic equations for rapid flows of smooth inelastic spheres, to burnett order. *J. Fluid Mech.* **361**, 41–74.

Serero, D. 2009 Kinetic theory of granular gas mixture. PhD thesis, Tel Aviv University.

Serero, D., Noskowicz, S. H., Tan, M. L. & Goldhirsch, I. 2009 Binary granular gas mixtures: Theory, layering effects and some open questions. *European Physical Journal-special Topics* **179**, 221–247.

Singh, C. & Mazza, M. G. 2018 Early-stage aggregation in three-dimensional charged granular gas. *Phys. Rev. E* **97**, 022904.

Singh, C. & Mazza, M. G. 2019 Electrification in granular gases leads to constrained fractal growth. *Sci. Reports* **9**, 9049.

Takada, S. & Hayakawa, H. 2018 Rheology of dilute cohesive granular gases. *Phys. Rev. E* **97**, 042902.

Takada, S., Saitoh, K. & Hayakawa, H. 2016 Kinetic theory for dilute cohesive granular gases with a square well potential. *Phys. Rev. E* **94**, 012906.

Takada, S., Serero, D. & Pöschel, T. 2017 Homogeneous cooling state of dilute granular gases of charged particles. *Phys. Fluids* **29**, 083303.

Watanabe, H., Ghadiri, M., Matsuyama, T., Ding, Y. L., Pitt, K. G., Maruyama, H., Matsusaka, S. & Masuda, H. 2007 Triboelectrification of pharmaceutical powders by particle impact. *Int. J. Pharm.* **334**, 149–155.

Yoshimatsu, R., Araújo, N. A. M., Wurm, G., Herrmann, H. J. & Shinbrot, T. 2017 Self-charging of identical grains in the absence of an external field. *Sci. Reports* **7**, 39996.